**ORIGINAL PAPER**

CrossMark

# Population-wide garnet growth zoning revealed by LA-ICP-MS mapping: implications for trace element equilibration and syn-kinematic deformation during crystallisation

F. R. George[1] · F. Gaidies[1] · B. Boucher[2]

## Abstract

The strong partitioning of many trace elements into garnet and their slow diffusivities in both garnet and the rock matrix means that their distribution may record valuable petrogenetic information not documented by major elements in metamorphic rocks. Complex trace element growth zoning in garnet porphyroblasts from a garnet-grade metapelite from the Barrovian sequence of the Sikkim Himalaya is assessed using quantified LA-ICP-MS raster mapping coupled with X-ray micro-computed tomography. The data document systematic changes in the zoning patterns from early- to late-nucleated crystals, and also suggest that the REE+Y chemistry incorporated into garnet is dependent on persistent disequilibrium in the rock volume. There is evidence for HREE+Y diffusion haloes surrounding growing garnets and a heterogeneous HREE+Y distribution in the rock matrix. Annuli superimposed on oscillatory zoning are not consistent with formation during some rock-wide event, but are dependent on the spatial disposition of the garnet. Annuli are interpreted to reflect an integrated history of varying growth rates and the incorporation of pre-existing heterogeneities due to relatively slow matrix diffusivities. Conversely, smooth zoning of many transition metals indicate that their distribution in garnet may be controlled by equilibrium partitioning between garnet and the rock matrix. Significant rotation of garnet porphyroblasts during growth is revealed due to immobility of Cr over the duration of the crystallisation interval and overprinting of the heterogenous precursor Cr distribution. Strain rate estimates derived from this zoning are on the order of $10^{-11}$–$10^{-12}$ s$^{-1}$.

**Keywords** Trace elements · Rare-earth elements · Garnet zoning · Crystal growth · Equilibrium · Spiral zoning · LA-ICP-MS

## Introduction

Metamorphic garnet is an invaluable tool in a petrologists arsenal, largely because of its chemical sensitivity to changing pressure and temperature (*P–T*) conditions over the duration of garnet crystallisation. The ability to reconstruct changing *P–T* by coupling the study of major element mineral chemistry and the principals of equilibrium thermodynamics has yielded great insight into both regional tectonic

Communicated by Jochen Hoefs.

✉ F. R. George
   freya.george@carleton.ca

[1] Department of Earth Sciences, Carleton University, Ottawa, Canada

[2] Department of Earth Sciences, University of New Brunswick, Fredericton, Canada

processes (e.g. Spear et al. 1984; Zhao et al. 2000; Catlos et al. 2001; Dasgupta et al. 2004), and our understanding of the grain-scale controls on metamorphic mineral crystallisation (e.g. Chernoff and Carlson 1997; Ague and Carlson 2013; George and Gaidies 2017).

While major element zonation developed in a garnet crystal during its growth continues to be informative, trace elements, particularly the rare-earth elements (REE), are generally thought to have order of magnitude slower diffusivities in both garnet and in the matrix compared to major elements (e.g. Cherniak 2005; Carlson 2012). Consequently, they are less susceptible to diffusional homogenisation and may record a more primary geochemical signature of garnet crystallisation not otherwise preserved by major elements. Owing in part to developments in laser ablation-inductively coupled-mass spectrometry (LA-ICP-MS) analytical capabilities and detection limits (e.g. Jackson et al. 1992; Norman et al. 1996; Heinrich et al. 2003; Woodhead et al. 2007;

Ulrich et al. 2009; Paul et al. 2012), trace element zonation within garnet has been shown to yield information pertaining to a range of metamorphic processes. For example, REE zoning has been used to shed light on accessory mineral reaction histories (e.g. Lanzirotti 1995; Pyle and Spear 1999; Yang and Pattison 2006), changes in the major phase assemblage over the duration of garnet crystallisation (e.g. Konrad-Schmolke et al. 2008), garnet resorption histories (Pyle and Spear 1999; Kohn and Malloy 2004), metamorphic fluid infiltration, and diffusion-limited uptake and trace element equilibration (Skora et al. 2006; Moore et al. 2013; Raimondo et al. 2017).

The primary incorporation and spatial distribution of trace elements in garnet has also been shown to have critical importance to Lu–Hf and Sm–Nd garnet ages, and on their tectonometamorphic implications (Skora et al. 2006, 2009; Kohn 2009; Kelly et al. 2011). While Anczkiewicz et al. (2012) and Smit et al. (2013) effectively assessed trace elements along line profiles in a range of garnet sizes, most studies pertain to the analysis of a single crystal. The two-dimensional (2D) distribution of trace elements in garnets of different sizes has the potential to yield information that improves our understanding of nucleation and growth mechanisms over the duration of metamorphic crystallisation. Additionally, the trace element distribution in garnet may yield information about their transport and distribution in the intergranular medium during this interval.

This study investigates the distribution of trace elements in metamorphic garnets that are representative of a rapidly crystallised garnet population in a metapelite from the Sikkim Himalaya. A LA-ICP-MS raster mapping technique is applied to reveal the complex and highly variable trace element patterns in this centrally sectioned population. These data, considered in conjunction with results of major element diffusion and thermobarometric modelling in George and Gaidies (2017), suggest a lack of equilibration of the intergranular medium with respect to the REE during garnet crystallisation. However a characteristic change in the REE distribution observed in each garnet of this study suggests that there was a change in the diffusive lengthscale of HREE+Y during crystallisation. Elements that are strongly partitioned in matrix phases remain immobile over the duration of garnet crystallisation, and have been used to provide direct estimates of the strain rates experienced by the sample during Barrovian metamorphism.

## Regional context and sample description

The Sikkim Himalaya, located in north-east India, comprises a well-documented ~ 15 km-wide inverted Barrovian metamorphic sequence with increasing grade towards the Main Central Thrust (MCT) zone (Mohan et al. 1989; Dasgupta

et al. 2009; Mottram et al. 2014b). The sequence is particularly well-developed in the Paleoproterozoic Daling Group of the Lesser Himalayan Sequence (LHS), in which peak metamorphic conditions of each Barrovian zone are interpreted to have been achieved approximately simultaneously at 13–10 Ma, after *c.* 6 Myr of Barrovian metamorphism (Catlos et al. 2004; Anczkiewicz et al. 2014).

The garnet-grade sample (sample 24-99) from the existing studies of Dasgupta et al. (2009), Anczkiewicz et al. (2014), Gaidies et al. (2015) and George and Gaidies (2017) was selected for further characterisation using 2D LA-ICP-MS raster mapping. The garnets in sample 24-99 are contained within a relatively well-foliated matrix comprising muscovite, primary chlorite, biotite, quartz and plagioclase, with accessory ilmenite, tourmaline, allanite, apatite and zircon. A full petrographic description of 24-99 is provided in George and Gaidies (2017), and only relevant details pertaining to the garnet population are duplicated here.

High-resolution X-ray micro-computed tomography (XR μ-CT) scanning of a rock volume of ca. 37 cm$^3$ shows that the garnet population comprises 8173 crystals that exhibit a log-normal crystal size distribution (CSD) with a skewness of 0.8 (Fig. 1a). Maximum and minimum grain radii are 0.71 mm and 0.053 mm respectively, and the mean garnet radius is 0.24 mm. Many crystals exhibit faceted surfaces, with minor retrogression to ragged chlorite along the rims of some crystals. Garnets contain curved to sigmoidal inclusion trails comprising aligned ilmenite, apatite, allanite and flattened quartz that are commonly continuous with the external foliation. No xenotime or monazite has been documented in the sample, neither in the matrix nor as inclusions in garnet.

Electron microprobe analysis (EPMA) on central-sections of numerous differently sized garnets representative of the CSD indicate that the major element compositional zoning of the population is largely concentric about the core and parallel to dodecahedral {011} planes (Fig. 1b, c). Mn exhibits typical prograde bell-shaped zoning, Mg and Fe are characterised by core-to-rim increases, and Ca content decreases broadly from core-to-rim. Ca zoning is dominantly controlled by broad core-to-rim partitioning along the *P–T* path, but patchy, short wavelength fluctuations in Ca (Fig. 1c) attest to its slower diffusivity in the rock matrix and greater affinity for maintaining disequilibrium (e.g. Chernoff and Carlson 1997). The population demonstrates a systematic change in core compositions from large to small crystals, and has been shown to be consistent with a model where major element equilibration is attained between garnet rims and the rock matrix during garnet crystallisation (Gaidies et al. 2008). The crystal size evolution of the population is in line with size-dependent interface-controlled growth kinetics (George and Gaidies 2017).

According to this model, progressive nucleation and growth of the garnet population occurred between ~ 520 °C,
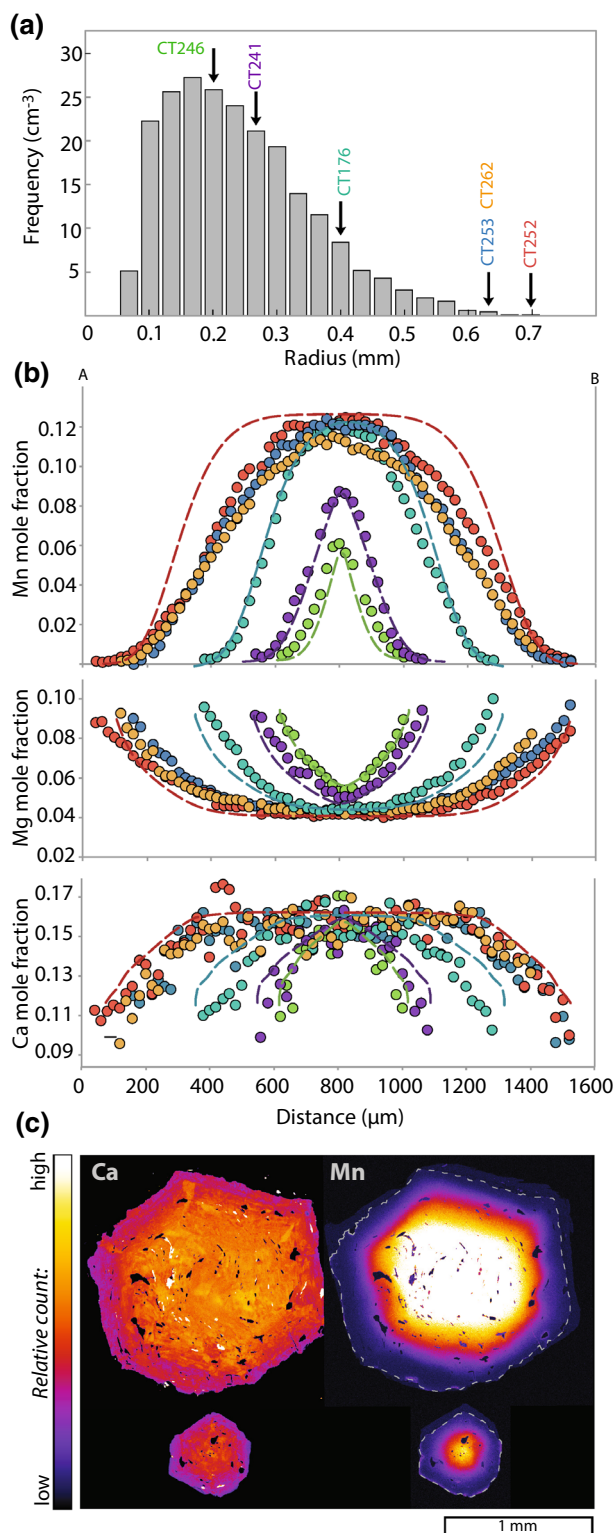
**Fig. 1 a** Crystal size-distribution for sample 24-99 as determined by μ-CT. Arrows indicate bins in which crystals have been mapped using LA-ICP-MS. **b** Mn, Mg and Ca EPMA zoning profiles for corresponding mapped garnets. Dashed lines are modelled garnets from George and Gaidies (2017). **c** Ca and Mn EPMA maps of largest (top) and smallest (bottom) segmented garnets

4.5 kbar and ∼ 565 °C, 5.5 kbar (George and Gaidies 2017). As shown in Fig. 1b, major element zoning of all garnets can be approximately predicted along this $P$–$T$ path for metamorphic heating rates in excess of 100 °C Myr$^{-1}$. Larger crystals have been shown to have nucleated early and small crystals nucleated later in the crystallisation history, with rapid successive nucleation of size classes 1–8 at approximately 520 °C. The model and radius-rate calculations suggest that large garnets have faster average radial growth rates than small garnets, with crystallisation of the whole population over < 1 Myr. The preservation of prograde growth zoning of Mn in the smallest crystals of the population, and the presence of compositional sector zoning in Fe and Ca along {211} crystal faces (Fig. 1c) similarly attests to a rapid average crystallisation history. Such rapid prograde evolution of the LHS is consistent with constraints from Anczkiewicz et al. (2014) and Mukhopadhyay et al. (2017), and is potentially related to elevated average radiogenic heat production in rocks from the Himalaya (Faccenda et al. 2008) or shear heating in the vicinity of the MCT zone (e.g. Le Fort 1975; Burg and Chen 1984; Mottram et al. 2014b), or both.

As a consequence of these rapid rates of metamorphic heating and resultant garnet growth at relatively low-$T$, the major elements in garnets of sample 24-99 have experienced negligible diffusional homogenisation during and subsequent to their growth. Thus, given the relatively simple prograde metamorphic history of the sample, investigation of the distribution of trace elements in garnet, coupled with the three-dimensional (3D) analysis of their size and spatial distribution may yield nuanced insight into the controls on trace element incorporation into metamorphic garnet and the extent of matrix equilibration during low- to mid-amphibolite facies regional metamorphism for a range of elements.

## Methods

### XR μ-CT

Sample 24-99 was imaged using the SkyScan 1173 high-resolution XR μ-CT facility at Carleton University, Ottawa, to spatially constrain the garnet distribution within the sample. Whole-rock scanning was conducted using a 130 kV/61 μA X-ray source and a 0.25 mm-thick brass filter, with an exposure time of 1300 ms. The sample was subsequently fragmented using the SelFrag disaggregation facility at Queen's University, Kingston, and garnets representative of the CSD were picked and mounted into grain mounts. These mounts were then each scanned at the XR μ-CT facility with a 70 kV/114 μA X-ray source, a 1300 ms exposure time and a 0.25 mm-thick aluminium filter, to permit accurate central sectioning of individual crystals.

SkyScan NRecon and Aviso software was used to render each XR μ-CT dataset into a 3D model, from which material statistics for the in situ and fragmented garnets were obtained. Comparison of geometric crystal-shape parameters between the two datasets allowed the identification of the spatial location of mounted garnets in the whole-rock dataset. Notably, the three large garnets analysed with LA-ICP-MS were in very close proximity in the scanned rock volume: 2.9 mm separates the geometric cores of crystals CT252 and CT253, and 4.6 mm separates crystals CT252 and CT262 (Fig. 2). CT252 and CT262 are situated in a common foliation plane, whereas CT253 is located in a parallel foliation plane approximately 3 mm away. Smaller analysed crystals could not be located in the whole rock dataset given their abundance in sample 24-99.

## Field-emission EPMA

Compositional maps of Y in garnet were obtained using a Cameca SX-5 electron microprobe equipped with a field-emission gun at the University of Vienna Department of Earth Sciences. Maps were produced using a focused acceleration voltage of 20 kV, a beam current of 100 nA, and a dwell time of 300 ms. Major element compositional maps (Fig. 1c) and Y maps both have a spatial resolution of 3 μm.

## LA-ICP-MS

LA-ICP-MS trace element maps were acquired using an ASI Resolution M-50 193 nm excimer laser ablation system housed at the University of New Brunswick Department of Earth Sciences. Ablation was conducted in a Laurin Technic Pty S-155 two-volume sample cell synchronised to an Agilent 7700x quadrupole inductively coupled plasma mass-spectrometer equipped with dual external rotary pumps.

Mapping was performed on six centrally sectioned garnet crystals (from CSD classes indicated in Fig. 1a), and was achieved by ablating a series of parallel rasters across the sample surface within a polygon defined by the garnet edges. Raster scans used a 17 μm crater with a 5 μm s$^{-1}$ stage scan speed, a laser pulse rate of 10 Hz and a ~ 3 J cm$^{-2}$ laser fluence. Ablation was performed in a mixed He (300 mL min$^{-1}$) and Ar (930 mL min$^{-1}$) carrier gas, which was mixed downstream with 2 mL min$^{-1}$ N$_2$ to enhance sensitivity. A dual rotary pump was used to double the spectrometer sensitivity to medium and heavy elements. Data acquisition was completed in a time-resolved analysis mode as a single continuous experiment for each garnet. Each experiment collected a suite of 34 elements (31 trace elements plus Si, Ca and Mn), a 15 s gas blank was run before each ablation line, and standards were measured approximately every 30 min. NIST610 was used as an external standard, with additional standards

NIST612 and USGS BCR2G (Pearce et al. 1997; Rocholl 1998).

Post-acquisition integrated scan lines were then generated offline using the internally standardised trace element data reduction scheme included in the *Iolite3*™ software package (Hellstrom et al. 2008; Paton et al. 2011), an add-in for Wavemetrics *Igor Pro v.6.32*™. Instrument drift and mass bias were corrected by applying a smoothed spline (spline smooth 2 in this study) along standards, and the average background was subtracted from each raster. Quantification of laser data was completed using an assumed stoichiometric value for Al in garnet (10.84 wt%), with accuracy of the analysis confirmed using NIST612 and USGS BCR2G. Trace element maps were subsequently visualised as fully-quantified ppm data using the CellSpace Image function in *Iolite*.

The trace element content was evaluated in relevant matrix phases using single spot LA-ICP-MS analysis. Spots utilised a 33 μm beam diameter, at 3 Hz using a 1.5 J cm$^{-1}$ laser fluence. Ablation was continuous for 40 s, with 30 s gas background. Carrier gases were as previously described.
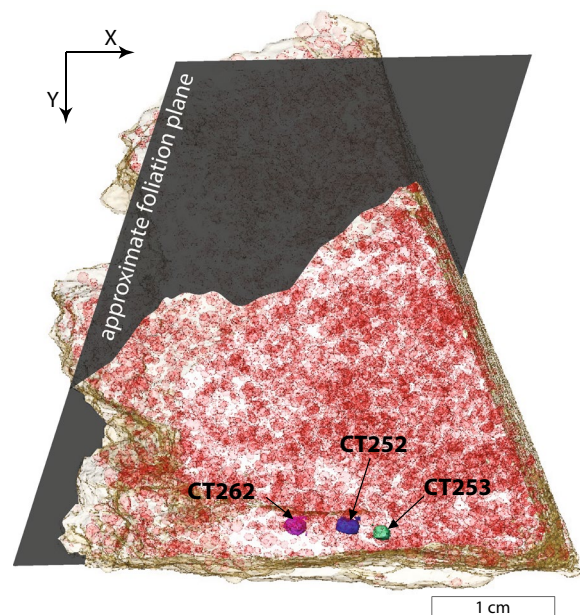


**Fig. 2** X–Y view of whole rock volume of sample 24-99 as scanned with μ-CT. The three largest garnets are highlighted (all other garnets in red), and the orientation of approximate foliation plane is illustrated

# Results

## Garnet chemical composition

From the suite of 31 trace elements collected for each of the six mapped garnet crystals, 24 of the most informative elements for CT252, CT253 and CT256 (the three largest garnets) are presented in Figs. 3, 4 and 5, respectively. Results from the remaining mapped crystals (CT176, CT241 and CT246) are available in Online Resource 1. Quantitative line profiles that best highlight the REE+Y zoning are shown in Fig. 6b–g. Note that the locations of these profiles do not correspond with major element lines in Fig. 1b.

### Heavy rare-earth elements and Y

Compositional zoning patterns of the HREE (Dy to Lu) and Y are decoupled from the smooth, relatively continuous zoning exhibited by the major elements in garnets from sample 24-99 (Fig. 1b, c). For ease of interpretation, major HREE+Y zoning features for each crystal are highlighted in Fig. 6a.

Garnets of all sizes exhibit a patchy-to-sigmoidal distribution of HREE+Y in their core regions, (Figs. 3, 4, 5, 6, 7a). At the chemical core of each crystal, concentrations generally reach their most extreme. There is a general progressive decrease in HREE+Y central peak concentration with decreasing crystal radius (with one exception, discussed below), and rim compositions are comparable for a given element in all crystals. Zoning of two of the largest crystals, CT252 and CT262 (with radii close to 700 μm) is very similar: ~ 1500 ppm Y, ~ 530 ppm Lu, ~ 2000 ppm Yb, ~ 120 ppm Tm, ~ 450 ppm Er, ~ 40 ppm Ho and ~ 60 ppm Dy in their central peaks. The core of the smallest analysed crystal contains ~ 400 ppm Y, < 10 ppm Lu, ~ 50 ppm Yb, < 10 ppm Tm, ~ 40 ppm Er, ~ 15 ppm Ho and ~ 50 ppm Dy. With decreasing atomic number, concentration maxima decrease, and elements with higher atomic numbers contain more significant relative concentration differences between the core compositions of large and small crystals (e.g. Lu compared to Ho, Fig. 8). Furthermore, HREE+Y are enriched in the cores of smaller garnets relative to their concentrations at the equivalent distance from the rims of larger garnets (Fig. 8).

In each garnet, patchy-to-sigmoidal cores are succeeded towards the rims by concentric HREE+Y oscillations approximately parallel to dodecahedral crystal surfaces (Figs. 3, 4, 5, 6, 7). Each garnet also contains several pronounced annuli that form sharp peaks at significantly higher concentrations than the background oscillations. Along a line profile within a given crystal, there is no spatial migration of the peaks according to atomic number, converse to

that observed by Skora et al. (2006) and Moore et al. (2013). There is no coincidence between the position of annuli and notable zoning features in the major elements, Zr or P. Li zoning is comparable to that of the HREE+Y, with evidence for concentric Li annuli surrounding an enriched core region (Figs. 3, 4, 5). This likely results from the coupling of Li to HREE+Y to maintain electroneutrality during element substitution (Cahalan et al. 2014).

Y and Mn contents were evaluated along distinct annuli within all six crystals (Fig. 9a), indicating that Y and Mn is approximately constant in concentration along the length of each annulus (subject to variations associated with raster direction versus profile direction and signal smearing). Similarly, the pyrope fraction at Y peaks along major element EMPA profiles in Fig. 1b shows approximate chemical symmetry about the elevated core (Fig. 9b). Figure 9a, b indicate that each annulus is compositionally distinct with respect to major and trace elements.

The geometries and relative locations of annuli in each crystal are variable, and crystals are therefore not easily comparable. The three annuli in CT252 are all located in close proximity to the rim, whereas in CT253 the annular transition is shifted towards the core (Fig. 9c). CT262 contains three irregular annuli similar to CT252, which have an orientation and structure at odds with the satellite peaks parallel to the dodecahedral surface situated towards the rims (Fig. 4). The latter forms annuli approximately parallel to present crystal interfaces, whereas the former is rotated relative to the present crystal surface. FE-EPMA maps of the largest garnet (CT252) indicate that the three dominant Y annuli (and by association, annuli of the other HREE) are characterised by sharp increases moving from core-to-rim, with a smoother decrease on the rim-ward side of each annulus (Fig. 7b).

CT253 is unique in that much of the relatively systematic, size-dependent trace element behaviour documented in other garnets is not present. Despite being of comparable radial size to the largest garnet, core compositions of the HREE+Y are similar to the magnitude of the smallest crystal, CT246: core Lu values in CT253 do not exceed 20 ppm (Fig. 8a), and Y reaches a maximum of ~ 300 ppm (Fig. 6d). However the particularly distinct annuli in CT253 are significantly more elevated relative to the core composition. Perhaps unexpectedly, major element zoning of this garnet is consistent with the systematic size-composition relationship documented within other crystals.

### Middle rare-earth elements and light rare-earth elements

There is inversion in the sense of zoning in the MREE compared with the HREE, with core-to-rim increases in the concentration of Gd, Sm and Eu, and a near homogeneous core-to-rim distribution of Tb. Unlike the significant size
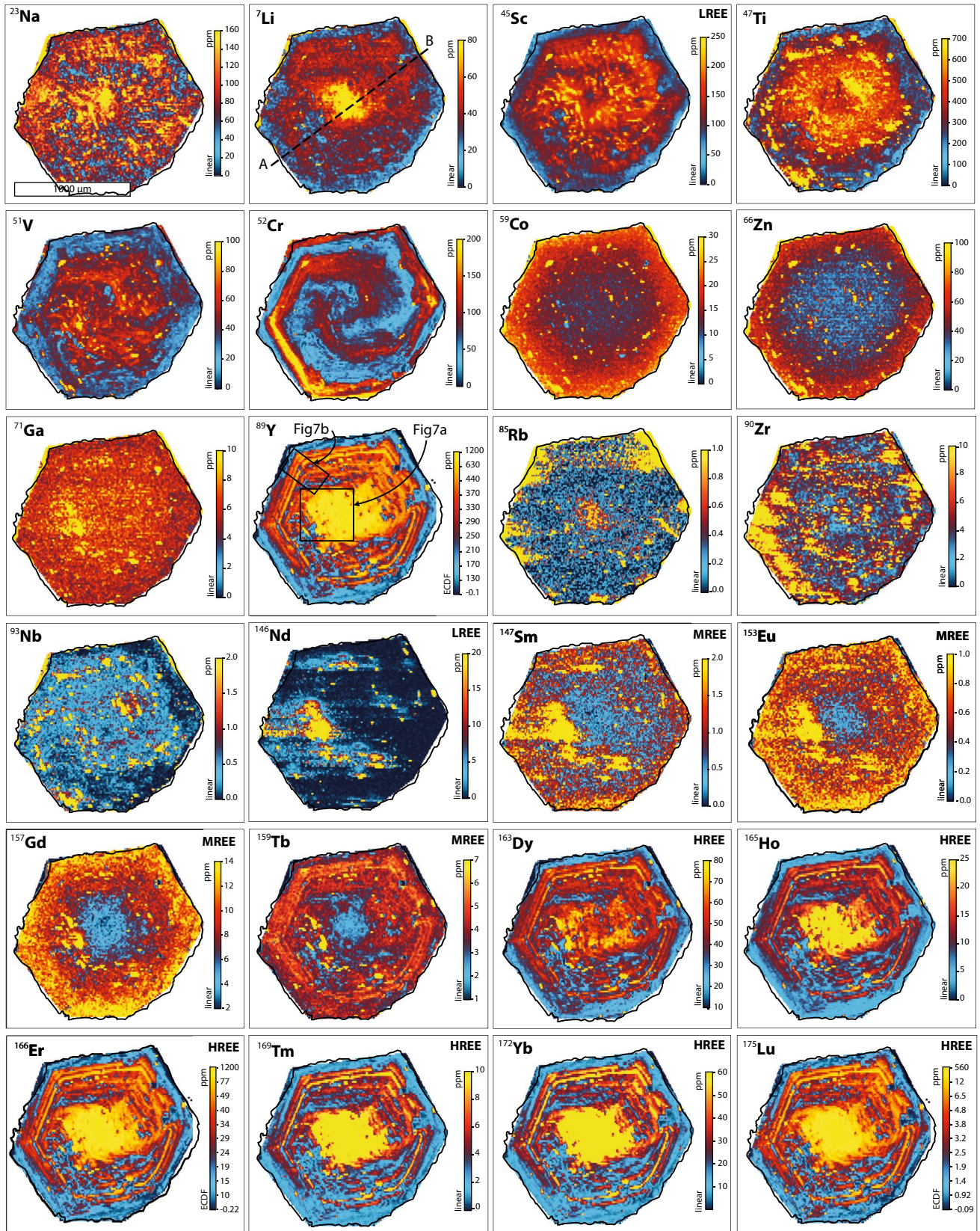
◀**Fig. 3** Selected quantified LA-ICP-MS raster maps for crystal CT252, the largest centrally sectioned garnet. All maps show ppm abundances with linear, log and ECDF scaling to accentuate zoning. Warmer colours indicate higher concentrations, and for the HREE+Y the maximum scaled value is saturated, such that the highest concentration exceeds the maximum scaled value. Line A–B shows the location of EPMA major element zoning traverse in Fig. 1b, boxes on Y map highlight location of Fig. 7. Raster direction is from left to right

dependence of the HREE, MREE zoning is less sensitive to crystal size, although some fractionation from large to small crystals is still notable in Gd. There are core-to-rim increases from ∼ 0.3 to ∼ 0.9–1.2 ppm and from ∼ 0.5 to ∼ 1.5 ppm for Eu and Sm, respectively (Fig. 6b–g). Gd is more notably zoned, with core compositions of 2–4 ppm and rims of 11–13 ppm in all garnets. Average Tb concentrations are approximately constant at 3–5 ppm from core-to-rim in all garnets.

Despite little systematic rim-to-rim zoning, Tb is the only MREE that shows evidence for pronounced compositional change that is spatially coincident with the position of HREE+Y annuli. Line profiles reveal that some correlative peaks and troughs are also present in Gd and Eu. Some MREE peaks are non-correlative with HREE features. Despite lower than anticipated HREE concentrations in CT253, the MREE do not exhibit any depletion relative to other similar-sized garnets.

Maps of light rare-earth elements (LREE: Ce, Pr and Nd) do not record any systematic crystallisation-related zoning, or are zoned at a scale less than detectable by LA-ICP-MS. LREE record the presence of accessory inclusions in the garnets as a series of saturated patches.

### Transition elements and other metals

Cr zoning is unique amongst the mapped elements: in all garnets Cr exhibits continuous spiral zoning that traverses from core-to-rim, with spirals centred on the compositional and geometric core of each crystal (Fig. 10). The zoning is defined by two approximately discrete regions: a high-Cr and a low-Cr domain. Low-Cr domains contain between 20 and 55 ppm Cr. Towards garnet rims, high-Cr zones become increasingly enriched, with values reaching 160 ppm Cr, compared to 100–120 ppm nearer the core (Figs. 3, 4, 5). CT176 has high- and low-Cr zones but does not document continuous spiral zoning, likely resulting from a poorly oriented section relative to the spiral geometry. Maps also show poorly defined oscillatory Cr zoning parallel to HREE+Y.

Spiral Cr zoning shows remarkable parallelism with the sigmoidal inclusion fabrics in garnet. As illustrated in Fig. 10, high-Cr zones strongly correlate with regions containing inclusions of ilmenite, allanite and apatite, whereas areas of low-Cr correspond almost exclusively to flattened quartz inclusions. This is the case in garnets of all sizes,

regardless of degree of apparent rotation. The orientation of these Cr spirals is also correlative with the sigmoidal patterns in HREE+Y core regions and the curved patchy zoning in Zr. Ca zoning towards garnet cores (Fig. 1c) also exhibits evidence for similar element distribution.

Sc, Ti and V each exhibit core-to-rim decreases in concentration, with approximately constant rim compositions between crystals for a given element. Cores of the four largest crystals contain 160–200 ppm Sc, whereas the smallest contains ∼ 100 ppm Sc. Ti allows for tracking of ilmenite inclusions in garnet. Each element approximately mimics the sigmoidal zoning observed in HREE and Cr, with a more patchy distribution.

Unlike the complex zoning exhibited by other trace elements, zoning of Co, Zn and Ga is relatively simple in crystals of all sizes, not dissimilar to major element zoning. For each element, rims are approximately within error between crystal sizes, and there is no correlation between Co, Zn and Ga and the HREE+Y annuli. Co and Zn are characterised by broad core-to-rim increases, from ∼ 10 ppm to 25 ppm Co and ∼ 30 to 65 ppm Zn in the largest crystals. There is also progressive elevation of core values from large to small crystals. Ga concentrations broadly decrease from core-to-rim, with a maximum of 4 ppm variation in the largest crystal.

### Matrix phase geochemistry

Table 1 displays the major and trace element contents of muscovite, biotite and chlorite in sample 24-99. Analyses are the average of multiple grains, with an associated ± 1σ error. Muscovite, biotite and chlorite contain < 0.02 ppm Y and HREE below detection limits. Instead, these phases are relatively enriched in transition metals. All contain approximately similar Sc contents (17, 11 and 20 ppm in muscovite, chlorite and biotite, respectively), whereas Cr and V are significantly more abundant (138 and 162, 134 and 105, and 213 and 203 ppm Cr and V in muscovite, chlorite and biotite, respectively). Sc, V and Cr vary significantly about mean values in each analysed phase, with the implication that the associated trace element contents of these phases are heterogeneous throughout the section.

Chlorite and biotite contain relatively high concentrations of Zn and Co (∼ 976 ppm and ∼ 656 ppm, and ∼ 147 ppm and ∼ 107 ppm, respectively). Chlorite, biotite and muscovite contain similar Ga concentrations (45–65 ppm). The scarce (∼ 6 vol%) plagioclase was not analysed with LA-ICP-MS, but is expected to be relatively enriched in LREE, Sr and Ba (e.g. Bea et al. 1994). Cr in plagioclase is generally < 10 ppm. Quartz was not analysed.
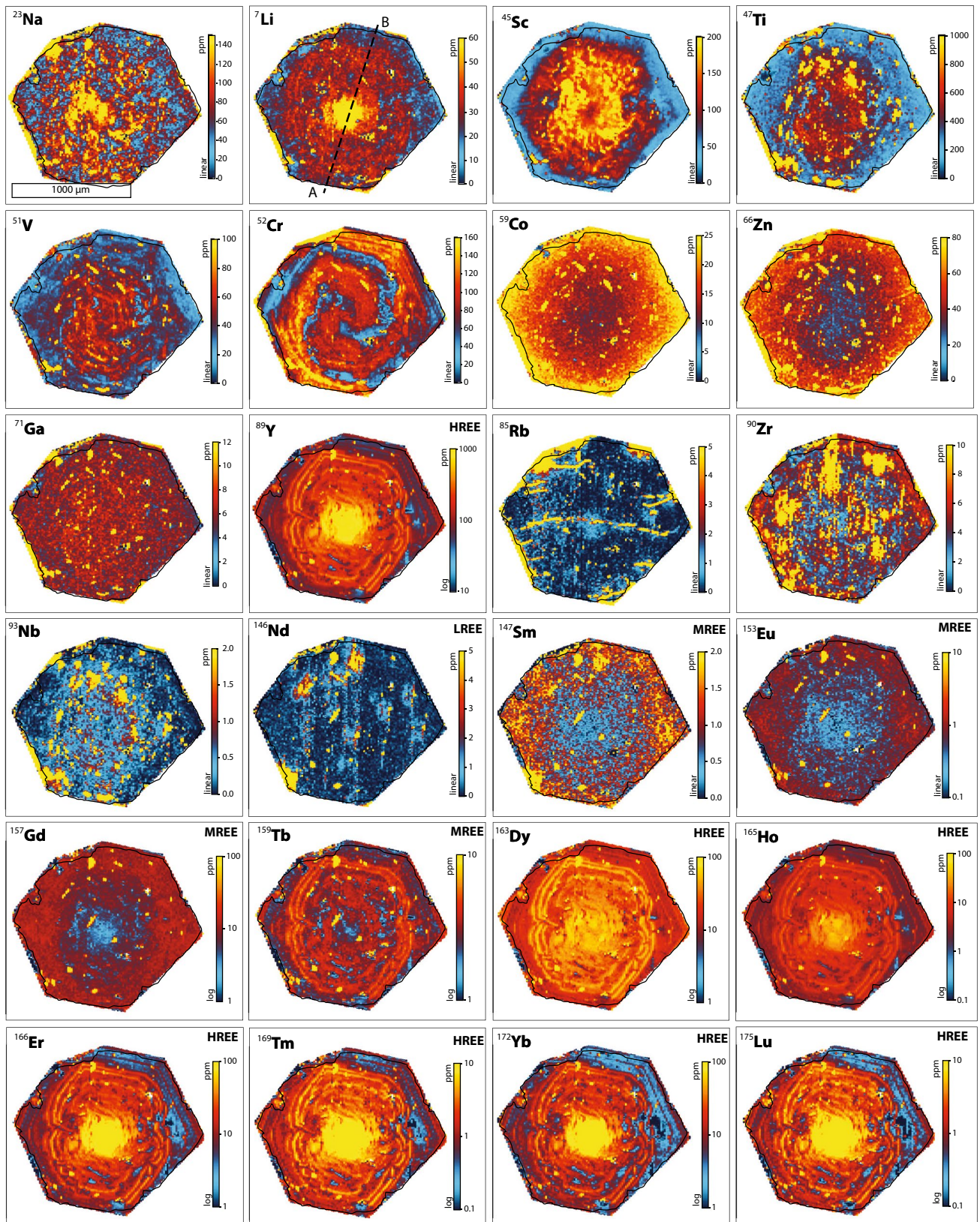
**Fig. 4** As Fig. 3 for crystal CT262. Raster direction is from south-southwest to north-northeast
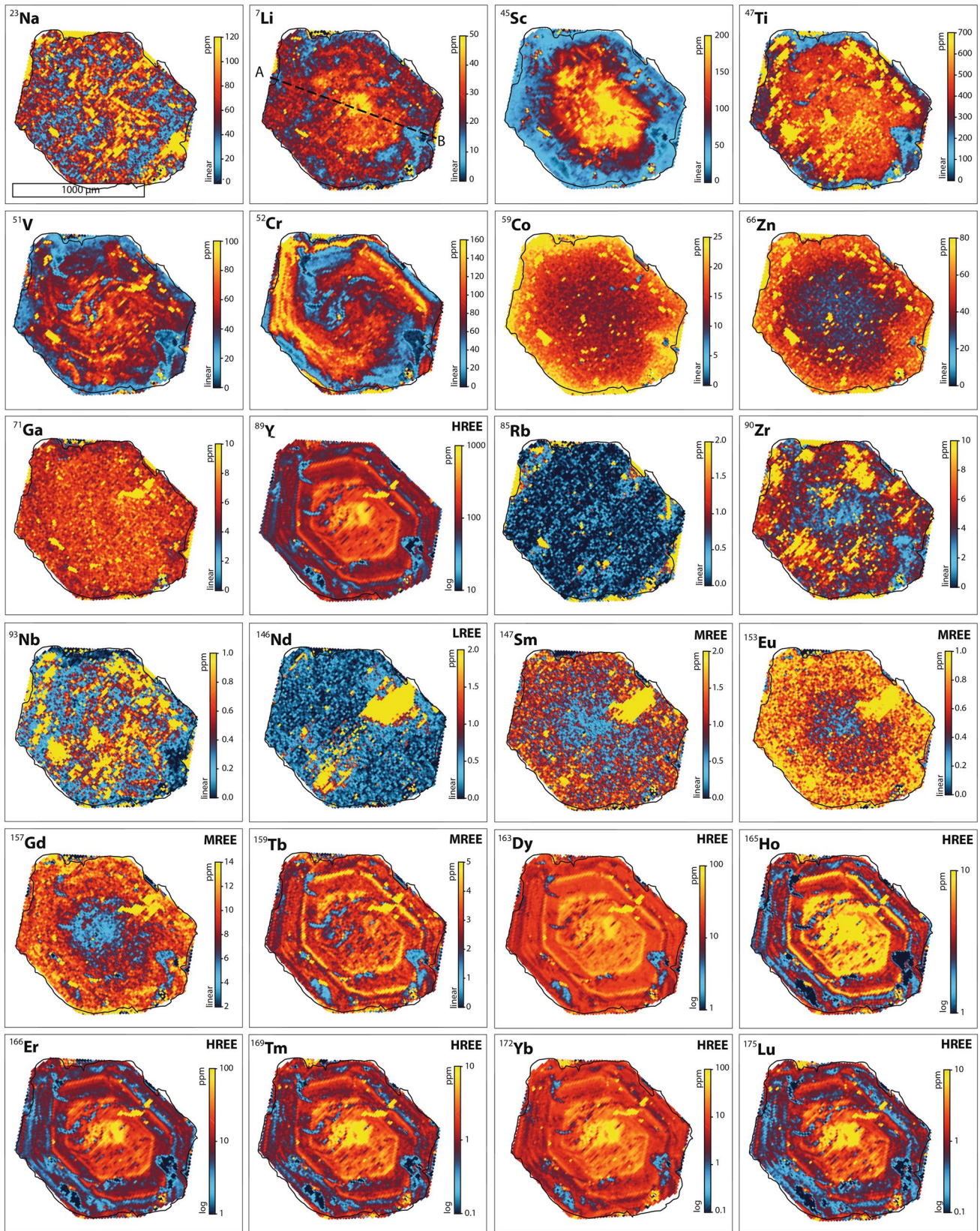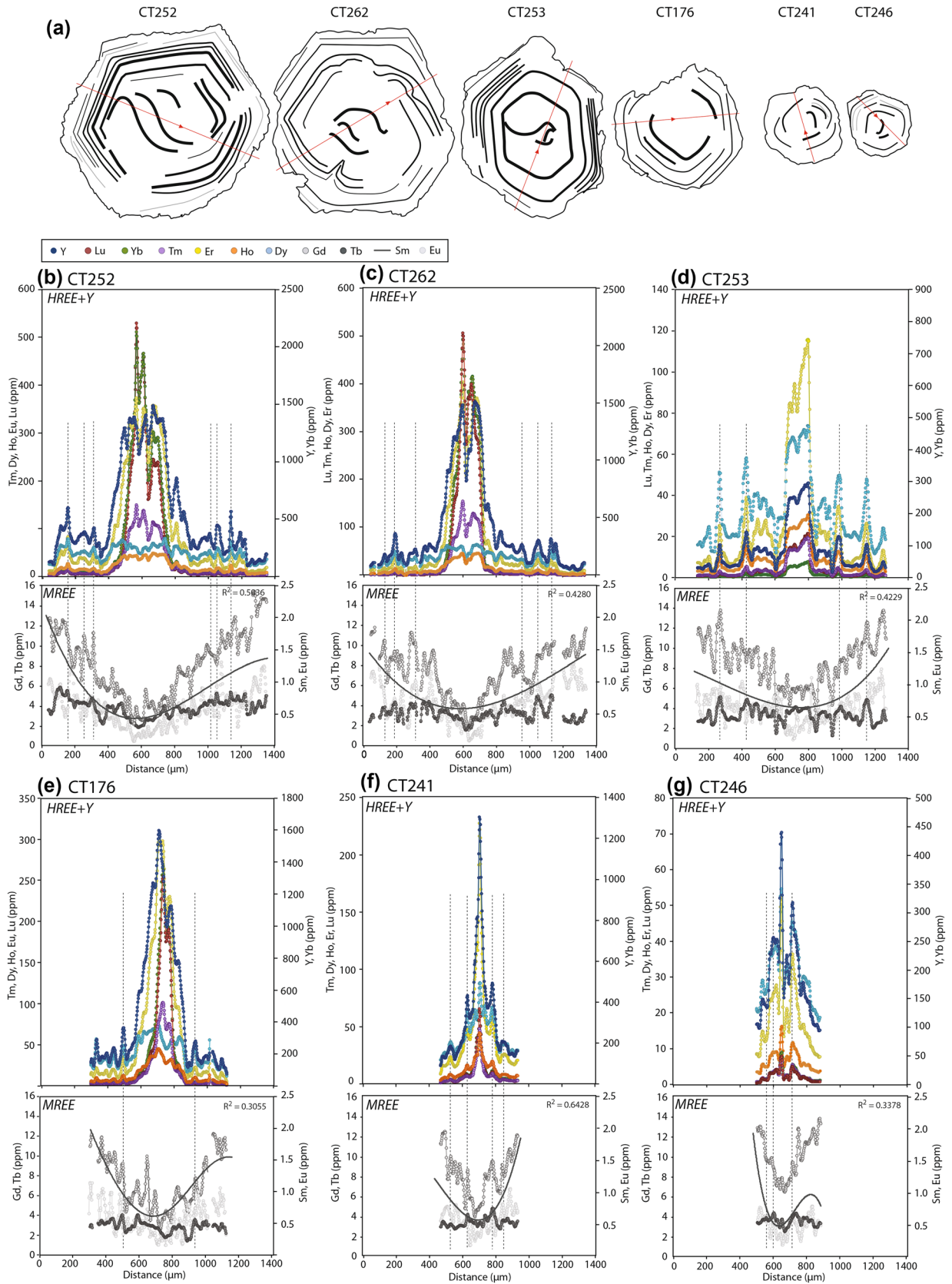
**Fig. 5** As Fig. 3 for crystal CT253. Raster direction is from southwest to northeast

◀**Fig. 6 a** Illustration of key HREE+Y zoning features exhibited by mapped garnets. Red lines denote line along which quantitative (ppm) profiles in **b**–**g** are collected. For each crystal, upper plot contains HREE+Y, and lower plot shows MREE. Note differential *y*-axis scaling in HREE+Y for differently crystals. Dashed vertical lines highlight alignment of element peaks

# Discussion

## Origins of trace element distribution

We focus our discussion on several phenomena documented in the trace element zoning patterns presented above. Namely, the influence of progressive garnet nucleation and growth on the trace element distribution in garnet, in relation to crystal size and extent of chemical equilibration of the rock matrix; the kinematic and textural controls on the sigmoidal-to-spiral Cr and HREE+Y zoning in garnet cores; and the formation mechanism of numerous concentric HREE+Y annuli. We also address the potential cause of the anomalous HREE compositions in garnet CT253.

## Size-dependent changes in zoning patterns

Similarities between the core compositions of similar-sized garnets CT252 and CT262 confirm their equivalent nucleation and early growth histories in regions of highest HREE, in a presumably undepleted precursor matrix. Patchy zoning in the cores of crystals suggests that during low-*T* growth, HREE+Y behaved in the same way as Ca (Menard and Spear 1996; Chernoff and Carlson 1997; Daniel and Spear 1998), with reduced mobility compared to Mn, Fe and Mg and a lack of hand sample scale equilibration. The curved patterns in the core HREE+Y zoning (particularly evident in the largest crystals) appear to have been partially inherited from the trace element distribution present in the pre-existing fabric that was overprinted during growth.

The strong enrichment of HREE in restricted core regions of each garnet (Fig. 6b–g) results from the fractionation of elements into the earliest formed portions of each garnet, with more pronounced enrichment for those elements with higher atomic numbers and partition coefficients. Coupled strong partitioning of HREE+Y into early-grown garnet and slow rates of diffusion in the matrix likely resulted in the development of a concentric diffusion halo with steep chemical potential gradients around each growing garnet in which the trace element concentration was depleted (e.g. see Carlson 2006). Despite the development of depletion haloes, core regions are generally characterised by irregular chemical patterns, a relict of some precursor chemical texture. Thus, the early-incorporated chemistry of each garnet is as

much controlled by the distribution of HREE, as the rate of their transport in the matrix.

As with the change in major element chemistry with crystal size, a general systematic change in the HREE+Y core compositions with size in the crystal population is further evidence of progressive nucleation and growth of large to small garnets. In addition to systematic changes in the absolute concentration of HREE+Y, the cores of small garnets are enriched relative to equivalent distances from the rims of larger crystals (Fig. 8). This is most notable for the heaviest HREE. Similar to Skora et al. (2006), this further confirms the presence of chemical concentration gradients in the matrix during garnet crystallisation, because each radial increment of late-nucleated smaller garnets grew contemporaneously with radial increments of early-nucleated larger garnets, as evinced by assessment of major element zoning (George and Gaidies 2017).

This relative core enrichment may be attributed to several different phenomena. Firstly, small garnets may have nucleated in an already partially depleted matrix if diffusion haloes around previously grown garnets overlapped. Estimates of the characteristic diffusional length scale of HREE transport (defined as $l = \sqrt{D_{eff}t}$, e.g. Darken and Gurry 1953) with effective matrix diffusivities, $D_{eff}$, on the order of $10^{-18}$ to $10^{-23}$ m$^2$ s$^{-1}$, do not exceed 1.5 mm at the modelled crystallisation timescales, $t$, of 0.5–1.5 Myr. While this is of a magnitude of the nearest-neighbour spacing of the final porphyroblast distribution, the relative scarcity of early-nucleated crystals would necessitate diffusion haloes at least an order of magnitude larger than this lengthscale, if they were to intersect and deplete the bulk matrix during the early stages of garnet crystallisation.

Alternatively, if slow diffusivities preclude diffusion haloes from overlapping and homogeneously depleting the average matrix chemistry during crystallisation, the progressive change in core concentration with garnet size requires there to have been a compositionally heterogeneous pre-existing matrix with respect to HREE+Y. The assumption of a chemically equilibrated low-*T* precursor seems implausible, given the dependence of the effective diffusivity on *T*, the chemical variability in mica and chlorite even after peak metamorphic conditions (Table 1), and overprint zoning in the cores of garnet. Progressive nucleation and growth of garnet in a patchy, non-equilibrated precursor medium is also supported by the fact that regions of highest HREE+Y in LA-ICP-MS maps do not converge in the geometric centre of annuli, and are often irregular in shape, despite approximate symmetry in line profiles.

In the case that the HREE+Y distribution in the matrix was heterogeneous and approximately immobile at *T*'s of garnet crystallisation, the systematic change in core HREE+Y concentrations with garnet size may imply that the HREE+Y distribution had some direct or indirect control on
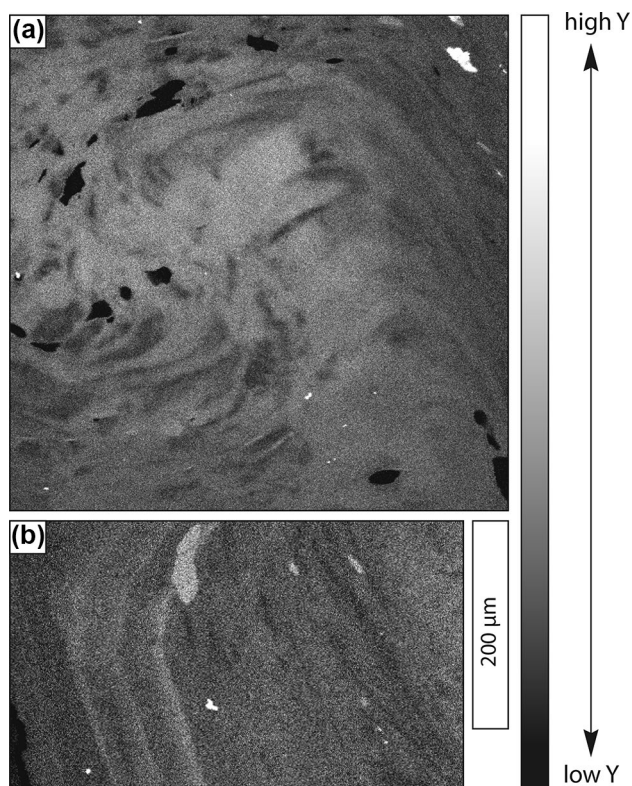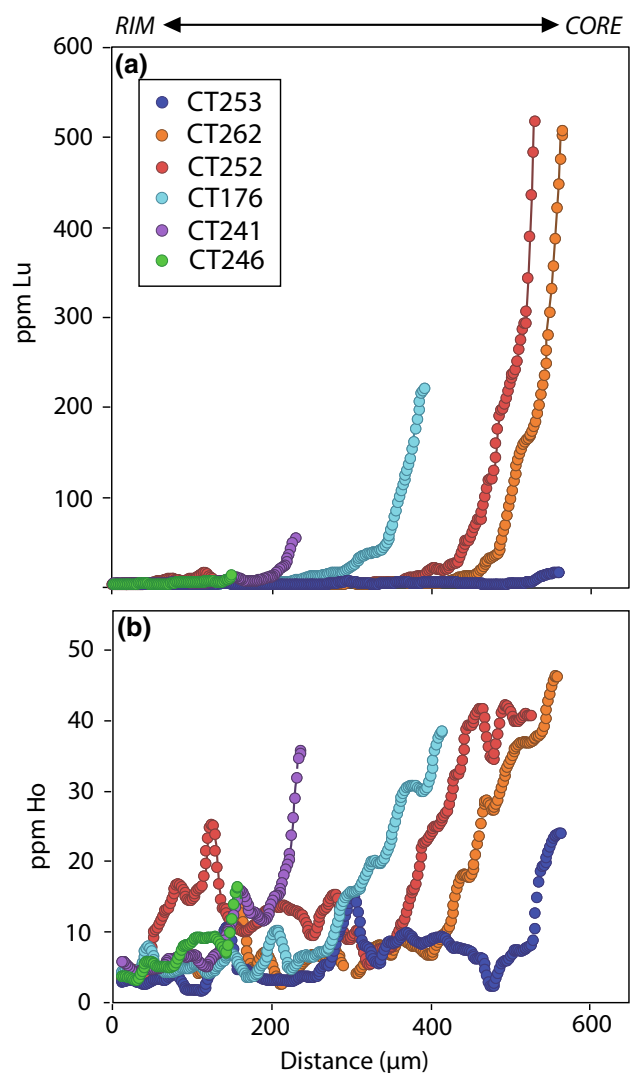
**Fig. 7** FE-EPMA maps of Y in the core (**a**) and rim (**b**) of garnet CT252. Mapped regions highlighted on LA-ICP-MS Y map (Fig. 3). Brighter colours denote high concentrations, dark colours indicate lower concentrations



**Fig. 8** Lu (**a**) and Ho (**b**) concentrations plotted against distance from rim for the mapped garnets. Core-rim concentration differences are larger for the heaviest REE (with the exception of CT253, see text for discussion)

the disposition of garnet nucleation sites. While it is generally well-established that trace elements are not an essential structural component in garnet, garnet may have preferentially nucleated in regions of highest HREE, with subsequent nucleation in sites of progressively decreasing HREE content. This population may, therefore, indicate that the trace element distribution and concentration may have had some impact on garnet nucleation, such that ease of nucleation scaled positively with the local concentration of HREE+Y.

While peaks and troughs are still present, the inverse core-to-rim MREE zoning does not show compositional change with crystal size to the extent documented by HREE+Y. This zoning can be attributed to the increasing incompatibility of MREE with decreasing atomic number (e.g. Bea et al. 1997; Kessel et al. 2005). Weak Tb zoning indicates garnet overprinted the bulk Tb distribution in the matrix rather than enhancing chemical potential gradients by strong fractionation. As a consequence, significant depletion haloes are unlikely to have developed for MREE.

As with major elements, the core contents of Co, Zn and Ga within smaller crystals correspond to concentrations of simultaneously grown rims in larger crystals. This, coupled with symmetrical smooth zoning of Co, Zn and Ga,

and progressive core variation with crystal size (similar to that observed in major element zoning) suggests potential equilibrium partitioning of these elements into garnet rims during growth. It is possible that the greater abundance and more widespread distribution of Co, Zn and Ga in matrix phases (Table 1) means that sample-wide equilibrium is more readily achieved for these elements in the matrix. Furthermore, the cationic radii of Ga, Zn and Co in both six- and eight-fold coordination is, on average, ~ 0.3–0.4Å smaller than the HREE (and similar to major elements), possibly facilitating an increased $D_{eff}$ through the grain boundary network and more effective chemical equilibration.

Broad core-to-rim changes in the concentrations of Co, Zn and Ga in garnet may also arise as a result of continuous adjustments to the garnet forming reaction over the duration
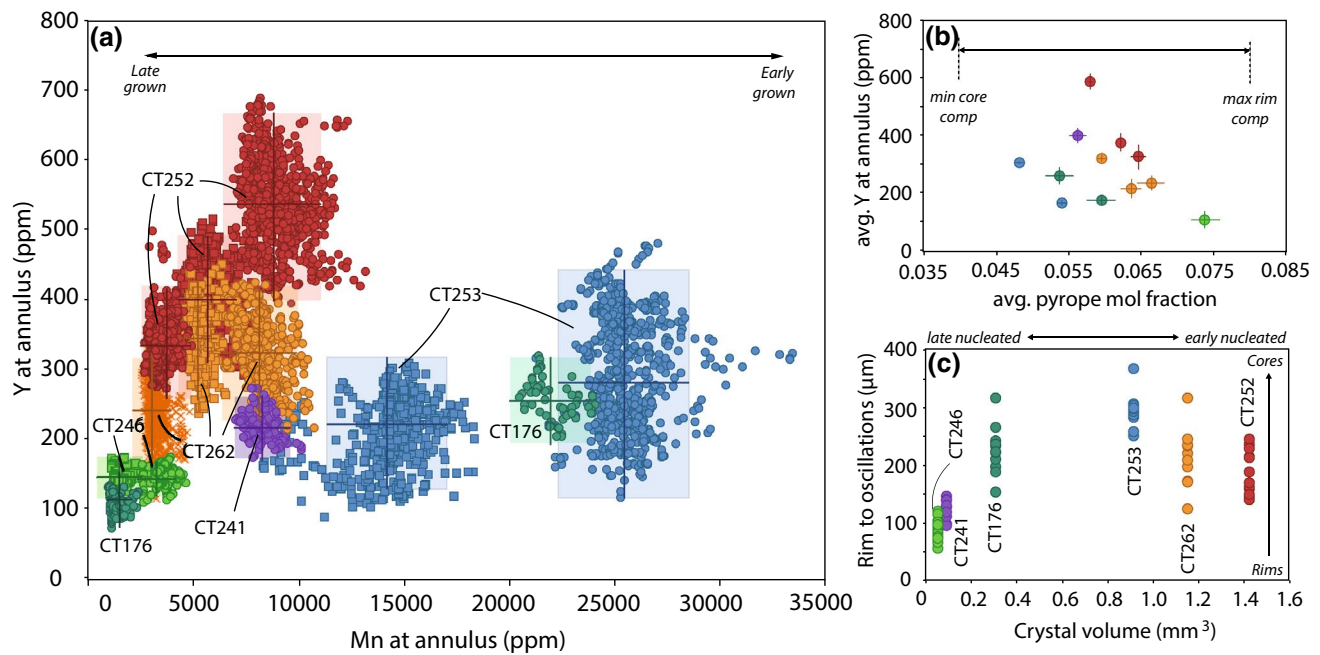
**Fig. 9 a** Mn concentration versus Y concentration along garnet annuli. Average and $\pm 2\sigma$ values for each annuli plotted as crosses. **b** Pyrope fraction versus Y concentration at annuli. Each point corresponds to averaged composition of LHS and RHS along major rim-to-rim profiles A–B, in Fig. 1b, with absolute variation plotted. **c** Measured distance from garnet rims to point at which HREE zoning becomes concentric, compared to absolute crystal volume (as measured with XR-μCT). Some scatter associated with measurement from numerous dodecahedral surfaces

of crystallisation. The broad zoning patterns observed in sample 24-99 are comparable to those in Raimondo et al. (2017), who suggested that progressive relative depletion and enrichment of the HREE and lighter elements, respectively, in remaining matrix minerals over the duration of garnet crystallisation can account for zoning patterns. While a gradual change in the compositions of the reacting phases is not able to account for the sharp peaks observed in HREE+Y, progressive relative enrichment of lighter trace elements and transition metals in remaining reactant phases, and their subsequent participation in the garnet-forming reaction may contribute to core-to-rim bowl shaped increases in some elements. Over the duration of garnet crystallisation, phase equilibria modelling indicates that modal abundance of plagioclase and chlorite decreased from 5 to 3 vol% and 14 to 10 vol%, respectively (George and Gaidies 2017), increasing the supply of Co and Ga (from chlorite in particular) towards the end of the growth sequence.

### Formation of spiral zoning

Precursor matrix foliations comprising alternating quartz–plagioclase microlithons and phyllosilicate-rich cleavage domains likely yielded alternating regions of relatively low- and high-Cr, respectively. Micas typically contain tens to hundreds of ppm Cr (Bea 1996; Yang et al.

1999; Yang and Rivers 2001; Pyle et al. 2001; Corrie and Kohn 2008; Janots et al. 2008), and our analysis indicates that muscovite, biotite and chlorite in sample 24-99 contain 100–240 ppm Cr, comparable to the concentration of Cr in high-Cr garnet domains. Petrographic assessment indicates that cleavage domains are also the predominant host of accessory phases, which may provide an additional source of Cr. Given the strong correlation between the inclusion populations and Cr content in garnet, it is inferred that the Cr distribution was controlled principally by the geometry of these precursor phyllosilicate layers. V and Sc distributions in garnet were likely also controlled by this strongly heterogeneous precursor rock texture.

Overprint Cr zoning has previously been documented in metapelitic garnets that have experienced conditions less than ~ 600 °C (Yang and Rivers 2001; Martin 2009; Raimondo et al. 2017). Cr in migmatitic garnets records concentric zoning, likely related to enhanced mobility of Cr at higher $T$ (Yang and Rivers 2001), or persistent disequilibrium between coexisting garnet and melt (Jung and Hellebrand 2006). Studies of amphibolite grade spiral Cr zoning in garnet has resulted in the widespread application of a model of garnet growth from two radial growth faces at a notch that remains approximately static in quartz pressure shadows as garnet grows and is rotated (Yang and Rivers 2001), to account for relatively high- to low-Cr zones.
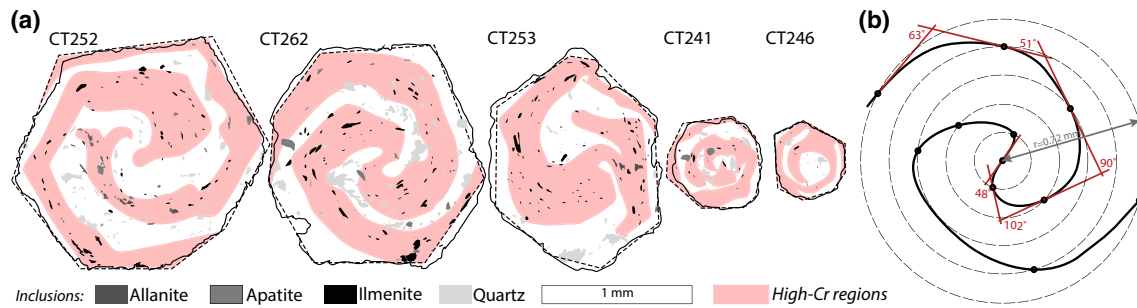
**Fig. 10** **a** Mapped inclusions of allanite, apatite, ilmenite and quartz, in addition to illustration of high-Cr regions in mapped garnets, in red. Solid lines denote edge of crystal and dashed lines indicate extent of LA-ICP-MS map. Garnet CT176 was not mapped with EMPA X-ray mapping, so inclusions cannot be definitively identi-fied. **b** Schematic sketch of spherical approximation of crystal CT262 showing average curvature. Intersects between average curvature and contours (black dots) were used to construct tangents to the curvature and calculate the angle of rotation (in red)

**Table 1** Matrix phase EPMA (wt%) and LA-ICP-MS (ppm) spot analyses

| n | Muscovite | | Chlorite | | Biotite | |
|---|---|---|---|---|---|---|
| | 14 | σ | 13 | σ | 7 | σ |
| (wt%) | | | | | | |
| SiO$_2$ | 47.70 | 0.12 | 24.83 | 0.05 | 36.19 | 0.11 |
| TiO$_2$ | 0.25 | 0.01 | 0.09 | n.d. | 1.52 | 0.04 |
| Al$_2$O$_3$ | 36.20 | 0.15 | 22.31 | 0.13 | 18.14 | 0.08 |
| FeO | 0.89 | 0.01 | 27.59 | 0.21 | 21.11 | 0.05 |
| MnO | 0.01 | n.d. | 0.05 | n.d. | 0.03 | n.d. |
| MgO | 0.58 | 0.03 | 12.27 | 0.11 | 8.43 | 0.04 |
| CaO | n.d. | n.d. | 0.03 | n.d. | 0.01 | n.d. |
| Na$_2$O | 1.79 | 0.06 | 0.07 | 0.01 | 0.23 | 0.01 |
| K$_2$O | 8.63 | 0.10 | 0.60 | 0.02 | 8.67 | 0.02 |
| Total | 96.05 | – | 87.84 | – | 94.33 | – |
| ppm | | | | | | |
| Li | 23.05 | 2.38 | 268.26 | 13.64 | 366.70 | 48.65 |
| Sc | 17.07 | 1.45 | 10.70 | 0.77 | 19.83 | 1.43 |
| V | 162.30 | 1.88 | 104.99 | 5.44 | 208.27 | 19.64 |
| Cr | 138.13 | 4.39 | 133.88 | 15.56 | 213.76 | 14.04 |
| Co | 5.66 | 1.42 | 147.40 | 6.40 | 107.36 | 11.29 |
| Zn | 44.70 | 10.55 | 976.08 | 47.27 | 655.97 | 69.95 |
| Ga | 52.51 | 0.75 | 61.45 | 47.27 | 45.51 | 4.86 |
| Rb | 354.56 | 10.92 | 72.03 | 40.78 | 1969.57 | 188.22 |
| Sr | 178.86 | 7.14 | 1.45 | 1.01 | 1.91 | 0.31 |
| Y | 0.02 | 0.01 | 0.01 | 0.01 | 0.02 | 0.01 |
| Zr | 0.10 | 0.02 | n.d. | n.d. | 0.03 | 0.01 |
| Nb | 13.85 | 0.27 | 3.18 | 0.99 | 80.46 | 7.83 |
| Cs | 3.99 | 0.47 | 6.54 | 4.16 | 115.71 | 19.78 |
| Nd | 0.01 | 0.01 | n.d. | n.d. | n.d. | n.d |
| Sm | n.d. | n.d. | n.d. | n.d. | n.d. | n.d. |
| Eu | 0.44 | 0.04 | n.d. | n.d. | n.d. | n.d. |

*n* number of analyses; ± 1σ standard deviation of the mean. LA-ICP-MS analyses for elements from Gd to Hf are excluded because all values are zero

*n.d.* not detected

However, coeval development of Cr spirals and concentric HREE+Y annuli preclude a non-concentric growth model in the garnet porphyroblasts from Sikkim. Instead, the partially decoupled zoning patterns indicate garnets underwent approximately concentric growth, with continued rotation over the duration of crystallisation.

Spirals and sigmoids defined by inclusion trails that formed during non-coaxial deformation have historically been interpreted to result from one of two end-member models: (1) rotation of porphyroblasts during growth due to significant coupling between the garnet and matrix interface (Rosenfeld 1970; Schoneveld 1977; Passchier et al. 1992), or (2) orthogonal reorientation of the external foliation around non-rotating porphyroblasts, in which deformation of the matrix is partitioned around the porphyroblast (e.g. Bell 1985; Bell and Johnson 1989; Hickey and Bell 1999). Although garnets have been isolated from their matrix in this study, the continuous Cr zoning strongly supports the former scenario, as there is little chemical evidence in garnet for the degree of misorientation of the matrix or of truncation of the internal foliation required by the non-rotational model. This kinematic record of continuous rotation during growth would not be evident from patterns of major elements or REE alone, which may otherwise suggest a cessation of rotation at conditions corresponding to the *P–T* of formation of the first annuli in each crystal.

Continuous spiral zoning from core-to-rim and lack of local chemical equilibration along the interface of growing garnet necessitates approximate immobility of Cr in the intergranular medium surrounding garnet during synkinematic growth. As discussed by Yang and Rivers (2001), Cr tends to become enriched in remnant phases due to its resistance to substitution reactions and relative insolubility in grain boundary fluids (Burns 1993), comparable to the immobile behaviour of Al in metapelites. The observation that Cr is unable to achieve even local equilibrium and preserves precursor Cr variations is therefore unsurprising. However, elevations of Cr towards the rims of crystals suggest either a gradual increase in the mobility of Cr parallel to pre-existing cleavage domains, or a progressive change in the partitioning of Cr into garnet with increasing *T*, or both. Slightly enhanced mobility of Cr at higher *T* is also supported by the presence of oscillatory Cr zoning parallel to {011} planes near garnet rims.

### Overprint to annular transition

In each mapped garnet the first annulus generally marks the transition from overprint zoning to concentric zoning parallel to the primary garnet-matrix interface. The concentric and linear nature of annuli is consistent with their formation during primary crystallisation, as opposed to forming in response to a resorption and regrowth episode (e.g. Pyle and Spear 1999; Kelly et al. 2011).

In the case that there was major element equilibration between garnet rims and the rock matrix, the concentrations of equilibrated components in garnet can be used as a relative timeline for garnet growth. The spessartine content is often used for such analysis (e.g. Finlay and Kerr 1979; Carlson 1989), and previous studies have used major elements to interpret annuli as rock-wide event markers, such that they formed at the same time in all crystals. However in an alternate case, Chernoff and Carlson (1997) concluded that Ca-spikes demonstrably did not form at the same time in all crystals, and are instead related to an event associated with the crystallisation history of each individual garnet crystal.

Equilibrium forward modelling of the garnet compositions and sizes in 24-99 yields a good fit for all major elements (George and Gaidies 2017). However, for large crystals, simulated concentrations of Mn in core regions are over-predicted (Fig. 1b), whereas the same compositions in small crystals are effectively reproduced. This may be attributed to uncertainties of equilibrium phase relations at low-*T* or spherical shape effects of the model, but may also point to a lack of equilibration of Mn between crystals during early growth, such that radial fractions grown at the same time incorporated different Mn concentrations. Thus, the use of Mn composition as a comparative timeline for annulus formation may be unreliable for garnets in 24-99. As Mg zoning is effectively reproduced by the modelling (Fig. 1b), the pyrope content in garnet may serve as an additional appropriate timeline. Given that rims of crystals are interpreted to have formed simultaneously, the distances from the rim to the most core-ward annulus can be used as a relative timeline for the transition from patchy zoning to concentric oscillatory zoning in different crystals.

As can be seen in Fig. 9a, b, characteristic annuli formed across a range of Mn, Mg and Y compositions (1500–26,000 ppm Mn, 0.046–0.075 mole fraction pyrope, and 110–520 ppm Y) and at a range of distances from crystal rims (Fig. 9c). Compositional constraints in Fig. 9a, b indicates that some annuli may have formed approximately simultaneously: a number of discrete annuli in different crystals formed at ~ 0.054, 0.060 and 0.065 mole fraction pyrope, and large crystals with similar element concentrations and modelled crystallisation histories (CT252 and CT262) contain comparable Mn at each of their annuli. This major element compositional correspondence between different annuli may point to their formation at similar times. However, there is by no means a systematic chemical trend throughout the population, making it unlikely that annuli are genetically related to some simultaneous event. Annuli that may have formed at comparable times display disparate Y concentrations, indicating a lack of chemical equilibrium for Y over the distances separating such crystals. Conversely, annuli with the same approximate Y contents formed at variable pyrope contents, further supporting a space- and

time-dependent HREE+Y distribution in the vicinity of each garnet.

There is no correlation between the major element concentrations in the cores of garnet and the Mn concentrations at the first annulus (as observed in Chernoff and Carlson 1997). Thus it is unlikely that there is a systematic relationship between the time of nucleation of a given crystal and the time at which its first annulus was generated. In other words, the annuli are not tied to the relative extent of the porphyroblastic reaction progress of individual crystals.

The lack of definitive correspondence between equilibrated major element chemistry at annuli in different garnets likely precludes their formation at the same time in some rock-wide event, or their systematic formation at a particular stage in each garnet's crystallisation history. While annuli are not rock-wide markers, the relative constancy of annuli composition along their lengths (Fig. 9a) and on either side of rim-to-rim compositional profiles (Fig. 9b) suggests that each given annulus is approximately equilibrated along its 2D length, and thus across the 3D surface of the growing garnet. The lack of HREE+Y equilibration in the vicinity of growing garnet, coupled with this continuous nature therefore necessitates some increase in the rate of grain boundary diffusion along the garnet surface at $P$–$T$ conditions of formation of the first annuli, relative to those conditions at which patchy zoning in garnet cores formed. Given the assumptions discussed, Fig. 9c indicates that CT252, CT253, CT262 and CT176 experienced this transition simultaneously, at a distance approximately 190–270 μm from crystal rims.

### Annuli formation mechanism

Discontinuous changes in Y and other REE contents in garnet have previously been ascribed to numerous formation mechanisms, including changing stability of major and accessory phases resulting in an increased availability of trace elements (Hickmott et al. 1987; Konrad-Schmolke et al. 2008; Moore et al. 2013); diffusion-limited uptake (Skora et al. 2006); infiltration of trace element enriched fluids (Hickmott and Spear 1992; Stowell et al. 1996); and disequilibrium partitioning in the vicinity of the interface and growth entrapment due to slow element diffusivities (e.g. Hickmott and Shimizu 1990; Lanzirotti 1995; Watson and Liang 1995; Watson 1996; Watson and Müller 2009). Given the caveats discussed pertaining to the HREE+Y distribution and relative timing of annuli formation, the applicability of these scenarios to the sample studied here are discussed below.

*Phase assemblage changes* Phase equilibria modelling and garnet-growth simulations coupled with detailed petrography indicate that the garnet population in 24-99 crystallised in a single graphitic assemblage containing muscovite, chlorite, quartz, plagioclase and ilmenite (George and Gaidies 2017). Consequently, discrete assemblage changes are not thought to be able to account for the observed changes in HREE+Y, as in the model of Konrad-Schmolke et al. (2008).

Pyle and Spear (1999) attributed shallow core-ward annulus gradients to progressive supply of HREE from discontinuous accessory phase reactions. However, steep compositional gradients on the core-ward side of annuli and shallow on the rim-ward side in 24-99 garnets (Fig. 7b) are inconsistent with a gradually increased supply of HREE and sudden decrease when the phase has reacted and the element supply is exhausted.

Regardless of the geometry of annuli, sample 24-99 is limited in its variance of trace element enriched accessory phases, with only ilmenite, zircon, apatite and allanite present in both the matrix and garnet. Neither monazite nor xenotime, both commonly saturated in HREE, are present and are hence considered unlikely candidates for the source of elevated HREE observed at annuli. While apatite can also act as a moderate sink for Y+REE (e.g. Heinrich et al. 1997), there is no notable variation in P in the garnets. No peaks are observed in LREE, making allanite an unlikely source of the HREE variation. Zircon breakdown would undoubtedly provide a significant source of HREE+Y to the advancing interface, but volumetrically significant release of Zr+HREE resulting from the dissolution of zircon in metapelites is unlikely to occur until the onset of partial melting (Kohn et al. 2015).

*Diffusion-limited uptake* The spatial correspondence of annuli of different HREE+Y in a given crystal, the geometry of the sharp peaks observed in the studied garnets, and the lack of annuli for the majority of MREE precludes the application of the diffusion-limited uptake model of Skora et al. (2006). While core HREE zoning trends are similar to those modelled by Skora et al. (2006), the growth of garnet in 24-99 may have occurred over too short a timescale to enable sufficient diffusion and re-enrichment of HREE in the vicinity of growing garnet to account for secondary peaks. In their model, a central peak only develops when the pre-exponential diffusion factor, $D_0$, is on the order of $10^{12}$–$10^{13}$ cm$^2$ year$^{-1}$, and rates of intergranular diffusion required for annular peaks to form are unrealistically rapid for the case of trace elements in 24-99.

*Fluid-mediated changes* The increased relative solubility of trace elements in metamorphic and metasomatic fluids yields the potential for significant fluxes of REE through a reacting rock during prograde metamorphism. As discussed by Haskin et al. (1966) and Hickmott et al. (1997), the solubility of HREE can be radically increased particularly in a F- or $CO_2$-rich fluid. However, the repeated nature of annuli would require multiple fluid infiltration events, yielding some cyclic heterogeneous fluid flux across the surfaces of

growing garnets. Repeated infiltration of fluids cannot be definitively ruled out, but there is no evidence for a compositionally distinct fluid or significant migration of fluid through the rock. Furthermore, mobility of major elements would similarly be expected to increase in a fluid-rich system. The success of major element simulations suggests that closed system behaviour closely approximates the effective bulk chemistry available during garnet growth.

*Growth entrapment and fluctuating growth rates* Given the evidence that the HREE+Y distribution in the matrix was not broadly equilibrated over the distances separating the analysed crystals during garnet growth, it can be expected that there were persistent regions of irregular HREE+Y content. Disequilibrium partitioning has previously been shown to be possible at the surface of a growing crystal due to near-surface enrichment or depletion of components with slow diffusivities (e.g. Hall 1953). Upon significant increases in growth rates, trace elements in the surface region can become bound in the surface layer, resulting in lattice concentrations that deviate from those expected with equilibrium partitioning. Preservation of such short-range compositional heterogeneity is dependent on the rate of interfacial advance relative to the rate of diffusion in the matrix and in the crystal: the ratio of diffusivity to growth rate is described by the growth Péclet number, and can be calculated as the product of the growth rate and lengthscale of diffusion, divided by the component diffusivity (e.g. Tiller 1991).

In a system defined by a high Péclet number (i.e. slow diffusion relative to growth rate), the rate of interfacial advance may exceed the rate of radial propagation of diffusion haloes, such that matrix heterogeneities are directly incorporated by growing garnet. Given the exceedingly rapid rates of radial growth predicted by our simulations, on the order of $10^{-19}$ m s$^{-1}$ (George and Gaidies 2017), this scenario is considered likely. Rapid garnet growth rates in 24-99 prevents significant equilibration of HREE+Y before heterogeneous matrix compositions are overprinted. However, unlike the apparently negligible diffusion in the intergranular medium, formation of annuli upon interface infringement of enriched or depleted zones in the matrix requires the diffusivity of HREE+Y parallel to the garnet-matrix interface have been extremely rapid, so as to allow for approximate equilibration along this 3D surface. Elevated *T*'s in the latter stages of growth (coupled with potential effects from changing element solubility in the grain boundary medium) may have facilitated this.

Minor fluctuations in the rate of radial garnet growth may also have had a dramatic effect on the compositional record of growth entrapment. As discussed by Watson and Müller (2009), for components with slow diffusivities, rapid mineral growth is expected to result in the accumulation of incompatible elements at the crystal-matrix interface. Conversely,

compatible elements are expected to be at a minima at the interface, and increasingly enriched into the matrix. Sudden discrete increases of an already rapid interfacial advance rate may result in the growth entrapment of the matrix concentration gradient in the new surface layer of garnet. This would yield a sharp core-ward side and a shallower gradient towards the rim, as is observed in 24-99 (Fig. 7b). However as compatible HREE are significantly enriched at annuli in garnets of 24-99, the increased growth rate model is not compatible with our observations.

Conversely, as suggested by Lanzirotti (1995) and as shown to be the case for MnO in garnet by Edmunds and Atherton (1971) and Burton et al. (1951), a decrease in the crystal growth rate will yield an increase in the concentration of compatible components at the surface of the growing crystal. For garnets in a heterogeneous matrix, discontinuous slowing of garnet growth could permit build up of compatible elements at the interface, and renewed rapid growth rates can subsequently overprint the elevated concentrations.

The oscillating nature of zoning towards the rims of garnets may therefore be associated with changes in growth rate. Phases of rapid growth will cause local depletion in trace element concentration, while a slowing of growth will allow build up of trace elements at the interface. Such changing growth rates may be driven by stepwise *P–T* changes, resulting from cyclic changes in slip rates along local faults (Kohn 2004). Shear motion in the vicinity of the MCT zone is commonly invoked to explain the rapid heating and metamorphic mineral growth in the Sikkim Barrovian sequence (e.g. Le Fort 1975; Burg and Chen 1984; Mottram et al. 2014b), and may have acted as an external driver of fluctuating garnet growth rates.

## Influence of rock texture on chemical zoning

While the systematic zoning of transition elements (excluding Cr) and the less abundant MREE may provide evidence for their approximate intergranular equilibration during mid-amphibolite facies metamorphism, persistent rock-wide disequilibrium with respect to HREE+Y is indicated by the irregularity of the zoning patterns. In addition to evidence for depletion haloes surrounding growing garnets, the variable form and timing of annuli development and the anomalous core composition of CT253 suggests that effective HREE bulk compositions may be significantly partitioned into a series of chemically distinct zones within 24-99. Cr also provides evidence of a strongly heterogeneous precursor rock texture.

The similarities between general zoning patterns and absolute concentrations of trace elements in CT252 and CT262 suggest a shared chemical history for some crystals. Micro-CT scans indicate that the cores of these crystals are separated by 4.6 mm within a shared foliation plane. It is

likely that the aforementioned garnets experienced similar crystallisation histories (i.e. with formation of annuli at approximately similar times) due to their distribution in an approximately similar chemical system, which must exist at least over the distance separating their cores.

Conversely, CT253 (which has a similar crystallisation history but exhibits unusually low HREE+Y concentrations and a contrasting annular pattern) is situated closer to CT252, but perpendicular to the foliation plane containing CT252 and CT262. Anisotropic intergranular diffusion in the rock matrix may therefore inhibit diffusive equilibration of HREE perpendicular to a spaced foliation, such that different local rock domains separated by as little as 4 mm contain significantly different HREE+Y concentrations, even prior to the onset of garnet growth. Micro-scale variations in effective bulk composition have been proposed previously (Stüwe 1997; Carlson 2002; Habler et al. 2009), resulting from differential diffusivities or strain induced heterogeneities. It may be the case that in 24-99, variations in the HREE+Y contents persisted in local domains defined largely by a strongly heterogeneous rock texture. Thus, the chemical system in which CT253 grew may have been dissimilar to that of CT252 and CT262, with respect to some elements only.

## Kinematics of porphyroblast rotation

Given the apparent continuity of porphyroblast rotation during growth, Cr spirals can be used to estimate strain rates that acted over the duration of garnet crystallisation. The lack of in situ matrix surrounding fragmented garnet precludes the calculation of strain rates in the non-rotational scenario (e.g. Berg et al. 2013), but internal fabrics can be used to derive estimates of strain rates for the porphyroblast rotation end-member case. This method follows that outlined by Biermeier and Stüwe (2003) and Berg et al. (2013), and relies on the relationship between strain rate and rotation,

$$\dot{\gamma} = \left( \frac{h}{\Delta T} \right) \times 2\omega, \tag{1}$$

where $\dot{\gamma}$ is the strain rate, $h$ is heating rate, $\Delta T$ is the change in temperature during a given interval of garnet growth, and $\omega$ is the magnitude of rotation over the interval. The crystallisation modelling of George and Gaidies (2017) provides a good basis for the variables required for this analysis. The correspondence between inclusion trails and inferred rotation-derived Cr spirals permits digital reslicing of single crystal μ-CT garnet datasets in order to evaluate the maximum inclusion curvature in the garnet crystals. In each case the plane showing the maximum curvature is approximately orthogonal to the elongation of the crystal. The amount of rotation, $\omega$, experienced by each crystal was constrained by measuring the angle between the tangential surfaces to the

average surface of rotation (Fig. 10b; Table 2). Equilibrium modelling of major element zoning has shown to be consistent with progressive nucleation of large to small crystals over the crystallisation interval. This allows approximate $P$–$T$–$t$ durations of growth of different crystal CSD size classes to be constrained. Volume–radius relationships for spherical crystals in our best-fit model require that early-formed growth zones grew exponentially more rapidly than late garnet shells, with a cumulative interval of ∼ 46 °C for core-to-rim growth of the largest garnet and ∼ 33 °C for the smallest analysed (see Fig. 11 of George and Gaidies 2017).

Diffusion modelling of major element zoning has yielded minimum heating rates of 100 °C Myr$^{-1}$ (George and Gaidies 2017). With the knowledge that diffusion modelling commonly yields minimum growth duration estimates (c.f. Viete and Lister 2016), this may represent the most rapid end-member of plausible rate estimates. A maximum duration of growth of 3.8 Myr derived from core and rim Lu–Hf geochronological constraints on a kyanite zone metapelite (Anczkiewicz et al. 2014) was used to place an upper end-member on the potential duration of garnet growth. For these calculations, a modified Eq. (1) was applied, as no $\Delta T$ was directly available.

For a constant heating rate of 100 °C Myr$^{-1}$, different crystal-integrated strain rate estimates are of a similar order of magnitude for large to small garnets: between $9.6 \times 10^{-12}$ s$^{-1}$ and $1.8 \times 10^{-11}$ s$^{-1}$. Average strain rates for the largest crystal is between $9.6 \times 10^{-12}$ s$^{-1}$ and $1.2 \times 10^{-13}$ s$^{-1}$, depending on the end-member rate chosen; the strain rate for the smallest crystal is between $1.8 \times 10^{-11}$ s$^{-1}$ and $1.7 \times 10^{-13}$ s$^{-1}$.

The apparent order of magnitude similarity of crystal-integrated strain rates is complicated given that small garnets nucleated after large garnets, but continued to grow with the same radial growth rate as larger ones for a given $P$–$T$ segment. The initial stages of garnet growth, recorded only in core regions of large, early-nucleated crystals, were much more rapid than later shared growth intervals (George and Gaidies 2017). In a simple case in which homogeneous strain operated over the whole rock volume, one would, therefore, expect late nucleated garnet to record less total $\omega$ than early nucleated ones, given the reduced $\Delta T$ over their

**Table 2** Strain rate calculations for garnet in sample 24-99

| Crystal | $\Delta T$ (°C) | $\omega$ (°) | $\dot{\gamma}$ (rad s$^{-1}$) | |
|---|---|---|---|---|
| | | | $h = 100$ °C Myr$^{-1}$ | d$r$/d$t$=3.9 mm Myr$^{-1}$ |
| CT252 | 46 | 398 | $9.59 \times 10^{-12}$ | $1.15 \times 10^{-13}$ |
| CT262 | 45.30 | 354 | $8.66 \times 10^{-12}$ | $1.03 \times 10^{-13}$ |
| CT253 | 45.30 | 260 | $6.36 \times 10^{-12}$ | $7.56 \times 10^{-14}$ |
| CT241 | 39.96 | 564 | $1.59 \times 10^{-11}$ | $1.67 \times 10^{-13}$ |
| CT246 | 37.00 | 599 | $1.79 \times 10^{-11}$ | $1.74 \times 10^{-13}$ |

crystallisation. The radial growth rate of earliest nucleated crystals over the initial 13 °C of their crystallisation was exceedingly rapid, with limited $\Delta t$ available for rotation. However, during the ~ 33 °C of shared history between the largest and smallest mapped crystals, objects might be expected to rotate simultaneously. This is not the case for garnets from 24-99; smaller crystals consistently contain larger $\omega$ than larger ones (Table 2). The lack of curvature correlation between objects partially growing at the same time therefore necessitates variable rotation operating over short length scales within the rock volume.

A textural and/or chemically irregular matrix is likely to result in a heterogeneous distribution of strain in the rock volume, yielding different apparent strain rates at the grain-scale. Large-scale variations in rotation may be explained by slight variations in shape or orientation of crystals (Passchier et al. 1992; Johnson et al. 2006; Johnson 2009), or the interactions between rigid objects in a deforming matrix (Ildefonse et al. 1992). Previous strain rate assessment (Barr and Houseman 1996; Biermeier et al. 2001; Biermeier and Stüwe 2003) has indicated the significant effect of porphyroblast texture on the rotation rate of cylindrical objects, and consequently, the calculated strain rate. The generalised relationship $\dot{\omega} \propto 0.5\,\dot{\gamma}$ (from Equation 1, where $\dot{\omega}$ is rotation rate) used is highly dependent on both the number and arrangement of rigid objects, and the boundary conditions of the system, and can vary between $\dot{\omega} \propto 0.25\dot{\gamma}$ and $\dot{\omega} \propto 0.75\dot{\gamma}$, depending on the porphyroblastic distribution (Biermeier and Stüwe 2003). Elevated strain rates in some cases can correlate with a change in rock chemistry, and may be the result of a metamorphic fluid that both modifies the chemistry and induces strain softening (e.g. Zulauf and Helferich 1997). Rocks in shear zones do not behave uniformly and most likely, the rheology of the matrix controls heterogeneous strain at the grain scale. Deformation partitioning into discrete zones of the matrix, each with variable components of simple shear may have yielded different deformation domains for different garnets (e.g. Bell 1985; Paterson and Vernon 2001; Griera et al. 2011).

The time-averaged strain rate estimates derived in this study for the garnet zone of Sikkim are an order of magnitude higher than previous indirect strain rate estimates from similar regionally metamorphosed terranes. Berg et al. (2013) used similar methods to derive strain rates on the order of $10^{-14}$ s$^{-1}$ for quartzose pelites from the Passo del Sole, and most regional strain rates are on the order of $10^{-15}$ to $10^{-13}$ s$^{-1}$ (e.g. Holm and Selverstone 1990; Müller et al. 2000; Biermeier and Stüwe 2003). While full treatment of the strain history and associated textural development is beyond the scope of this discussion, our $10^{-13}$ to $10^{-12}$ s$^{-1}$ strain rate estimates in Sikkim are broadly in agreement with those derived using piezometer by Ghosh et al. (2016), on rocks associated with motion along the Rangit Thrust. In Sikkim the location of both the MCT zone and the Rangit Thrust is highly contested (e.g. Catlos et al. 2004; Mottram et al. 2014a; Bose et al. 2014), but a zone of pervasive deformation is likely to persist through the Daling group Barrovian sequence. In fact, Bhattacharyya (2010) and Bhattacharyya and Mitra (2009) mapped the southernmost extent of MCT deformation (their MCT2) at the approximate collection location of 24-99, and calculated strain rates on the order of $10^{-12}$ s$^{-1}$ at this locale (Bhattacharyya and Mitra 2011).

## Conclusions

LA-ICP-MS maps of numerous garnets representative of a single rapidly crystallized population shed further light on the significant variability of the trace element distribution both within garnet, and in the intergranular medium from which garnet crystallised. Our work suggests that garnets from the Sikkim Barrovian sequence contains an integrated record of the interplay between variable element equilibration, changing garnet growth rates and rock deformation, which would go otherwise unobserved with major element analysis alone.

During the early stages of garnet growth, HREE+Y exhibit a lack of rock-wide equilibration and a strongly space- and time-dependent element distribution. This immobility, coupled with relatively slow diffusivities in garnet yields compositional mimicry of the pre-existing matrix in the cores of garnets. Conversely, some transition elements with greater matrix abundance exhibit approximate equilibrium behaviour, in part due to the shorter relative length scales required for homogenisation. Progressive change in core chemistry from large to small crystals attests to a progressive nucleation history, and may also point to preferential nucleation of garnet in HREE+Y enriched regions. The transition from overprint to oscillatory zoning necessitates an increase in the length-scale of equilibration of HREE+Y along the garnet–matrix interface during the crystallisation interval. The timing and formation mechanism of these annuli is not systematic through the rock volume, but is likely a function of the interplay between inhomogeneous growth rates, the incorporation of pre-existing heterogeneities due to slow matrix diffusivities and rapid growth rates, and the influence of domainal HREE+Y bulk chemistries.

The crystallisation dynamics of syn-kinematic garnet are revealed by the compositionally defined internal foliation, which is most evident in the core-to-rim spiral zoning of Cr. Coeval development of spiral Cr and concentric REE growth zoning necessitates the approximately concentric growth of garnet porphyroblasts during continued garnet rotation, and a strongly heterogeneous but layered Cr distribution in the precursor matrix. Spiral zoning has proven to be well-suited

to strain rate calculations: using thermobarometric and temporal constraints derived by George and Gaidies (2017), we derive an average strain rate from $10^{-11}$ to $10^{-12}$ s$^{-1}$, with significant sample-wide variation attributable to deformation partitioning in a texturally and microstructurally heterogeneous rock volume.

Persistent HREE+Y disequilibrium in a sample that may be otherwise considered an archetypal prograde garnet population highlights the need for caution when using non-equilibrated trace elements for geochronological or geothermobarometric studies. Until the spatial distribution of trace elements in garnet populations is better understood, thorough investigation of each sample is required to prevent misinterpretation of single garnet chemistries. Our study highlights the wealth of information that extensive datasets can provide to continue to improve our understanding of trace element distributions and garnet porphyroblast crystallisation.

# References

Ague JJ, Carlson WD (2013) Metamorphism as garnet sees it: the kinetics of nucleation and growth, equilibration, and diffusional relaxation. Elements 9(6):439–445

Anczkiewicz R, Thirlwall M, Alard O, Rogers NW, Clark C (2012) Diffusional homogenization of light REE in garnet from the Day Nui Con Voi Massif in N-Vietnam: implications for Sm-Nd geochronology and timing of metamorphism in the Red River shear zone. Chem Geol 318:16–30

Anczkiewicz R, Chakraborty S, Dasgupta S, Mukhopadhyay D, Kołtonik K (2014) Timing, duration and inversion of prograde Barrovian metamorphism constrained by high resolution Lu-Hf garnet dating: a case study from the Sikkim Himalaya, NE India. Earth Planet Sci Lett 407:70–81

Barr TD, Houseman GA (1996) Deformation fields around a fault embedded in a non-linear ductile medium. Geophys J Int 125(2):473–490

Bea F (1996) Residence of REE, Y, Th and U in granites and crustal protoliths; implications for the chemistry of crustal melts. J Petrol 37(3):521–552

Bea F, Pereira M, Stroh A (1994) Mineral/leucosome trace-element partitioning in a peraluminous migmatite (a laser ablation-ICP-MS study). Chem Geol 117(1–4):291–312

Bea F, Montero P, Garuti G, Zacharini F (1997) Pressure-dependence of rare earth element distribution in amphibolite-and granulite-grade garnets. A LA-ICP-MS study. Geostand Geoanal Res 21(2):253–270

Bell T (1985) Deformation partitioning and porphyroblast rotation in meta-morphic rocks: a radical reinterpretation. J Metamorph Geol 3(2):109–118

Bell T, Johnson S (1989) Porphyroblast inclusion trails: the key to orogenesis. J Metamorph Geol 7(3):279–310

Berg C, Carlson W, Connelly J (2013) Strain rates at high temporal resolution from curved inclusion trails in garnet, Passo del Sole, Central Swiss Alps. J Metamorph Geol 31(3):243–262

Bhattacharyya K (2010) Geometry and kinematics of the fold-thrust belt and structural evolution of the major Himalayan fault zones in the Darjeeling—Sikkim Himalaya, India. Ph.D. thesis, University of Rochester

Bhattacharyya K, Mitra G (2009) A new kinematic evolutionary model for the growth of a duplex—an example from the Rangit duplex, Sikkim Himalaya, India. Gondwana Res 16(3):697–715

Bhattacharyya K, Mitra G (2011) Strain softening along the MCT zone from the Sikkim Himalaya: relative roles of quartz and micas. J Struct Geol 33(6):1105–1121

Biermeier C, Stüwe K (2003) Strain rates from snowball garnet. J Metamorph Geol 21(3):253–268

Biermeier C, Stüwe K, Barr T (2001) The rotation rate of cylindrical objects during simple shear. J Struct Geol 23(5):765–776

Bose S, Mandal N, Acharyya S, Ghosh S, Saha P (2014) Orogen-transverse tectonic window in the Eastern Himalayan fold belt: a superposed buckling model. J Struct Geol 66:24–41

Burg J, Chen G (1984) Tectonics and structural zonation of southern Tibet, China. Nature 311(5983):219–223

Burns RG (1993) Mineralogical applications of crystal field theory, vol 5. Cambridge University Press, Cambridge

Burton W-K, Cabrera N, Frank F (1951) The growth of crystals and the equilibrium structure of their surfaces. Philos Trans R Soc Lond A Math Phys Eng Sci 243(866):299–358

Cahalan RC, Kelly ED, Carlson WD (2014) Rates of Li diffusion in garnet: coupled transport of Li and Y+REEs. Am Mineral 99(8–9):1676–1682

Carlson WD (1989) The significance of intergranular diffusion to the mechanisms and kinetics of porphyroblast crystallization. Contrib Mineral Petrol 103(1):1–24

Carlson WD (2002) Presidential address. Scales of disequilibrium and rates of equilibration during metamorphism. Am Mineral 87(2–3):185–204

Carlson WD (2006) Dana lecture. Rates of Fe, Mg, Mn, and Ca diffusion in garnet. Am Mineral 91(1):1–11

Carlson WD (2012) Rates and mechanism of Y, REE, and Cr diffusion in garnet. Am Mineral 97(10):1598–1618

Catlos E, Harrison TM, Kohn MJ, Grove M, Ryerson F, Manning CE, Upreti B (2001) Geochronologic and thermobarometric constraints on the evolution of the Main Central Thrust, central Nepal Himalaya. J Geophys Res Solid Earth 106(B8):16177–16204

Catlos E, Dubey C, Harrison T, Edwards M (2004) Late Miocene movement within the Himalayan Main Central Thrust shear zone, Sikkim, north-east India. J Metamorph Geol 22(3):207–226

Chernoff C, Carlson W (1997) Disequilibrium for Ca during growth of pelitic garnet. J Metamorph Geol 15(4):421–438

Cherniak DJ (2005) Yb and Y diffusion in grossular garnet. Geochimica et Cosmochimica Acta Suppl 69:A405

Corrie SL, Kohn MJ (2008) Trace-element distributions in silicates during prograde metamorphic reactions: implications for monazite formation. J Metamorph Geol 26(4):451–464

Daniel CG, Spear FS (1998) Three-dimensional patterns of garnet nucleation and growth. Geology 26(6):503–506

Darken LS, Gurry RW (1953) Physical chemistry of metals. CBS Publishers and Distributors, New Delhi

Dasgupta S, Ganguly J, Neogi S (2004) Inverted metamorphic sequence in the Sikkim Himalayas: crystallization history, P–T gradient and implications. J Metamorph Geol 22(5):395–412

Dasgupta S, Chakraborty S, Neogi S (2009) Petrology of an inverted Barrovian sequence of metapelites in Sikkim Himalaya, India: constraints on the tectonics of inversion. Am J Sci 309(1):43–84

Edmunds W, Atherton M (1971) Polymetamorphic evolution of garnet in the Fanad aureole, Donegal, Eire. Lithos 4(2):147–161

Faccenda M, Gerya TV, Chakraborty S (2008) Styles of post-subduction collisional orogeny: influence of convergence velocity, crustal rheology and radiogenic heat production. Lithos 103(1–2):257–287

Finlay CA, Kerr A (1979) Garnet growth in a metapelite from the Moinian rocks of northern Sutherland, Scotland. Contrib Mineral Petrol 71(2):185–191

Gaidies F, De Capitani C, Abart R (2008) THERIA\_G: a software program to numerically model prograde garnet growth. Contrib Mineral Petrol 155(5):657–671

Gaidies F, Petley-Ragan A, Chakraborty S, Dasgupta S, Jones P (2015) Constraining the conditions of Barrovian metamorphism in Sikkim, India: P-T-t paths of garnet crystallization in the Lesser Himalayan Belt. J Metamorph Geol 33(1):23–44

George F, Gaidies F (2017) Characterisation of a garnet population from the Sikkim Himalaya: insights into the rates and mechanisms of porphyroblast crystallisation. Contrib Mineral Petrol 172(7):57

Ghosh S, Bose S, Mandal N, Dasgupta S (2016) Dynamic recrystallization mechanisms and their transition in the Daling Thrust (DT) zone, Darjeeling–Sikkim Himalaya. Tectonophysics 674:166–181

Griera A, Bons PD, Jessell MW, Lebensohn RA, Evans L, Gomez-Rivas E (2011) Strain localization and porphyroclast rotation. Geology 39(3):275–278

Habler G, Thöni M, Grasemann B (2009) Cretaceous metamorphism in the Austroalpine Matsch Unit (Eastern Alps): the interrelation between deformation and chemical equilibration processes. Mineral Petrol 97(3–4):149

Hall R (1953) Segregation of impurities during the growth of germanium and silicon. J Phys Chem 57(8):836–839

Haskin LA, Wildeman TR, Frey FA, Collins KA, Keedy CR, Haskin MA (1966) Rare earths in sediments. J Geophys Res 71(24):6091–6105

Heinrich W, Rehs G, Franz G (1997) Monazite-xenotime miscibility gap thermometry. I. An empirical calibration. J Metamorph Geol 15(1):3–16

Heinrich C, Pettke T, Halter W, Aigner-Torres M, Audétat A, Günther D, Hattendorf B, Bleiner D, Guillong M, Horn I (2003) Quantitative multi-element analysis of minerals, fluid and melt inclusions by laser-ablation inductively-coupled-plasma mass-spectrometry. Geochim Cosmochim Acta 67(18):3473–3497

Hellstrom J, Paton C, Woodhead J, Hergt J (2008) Iolite: software for spatially resolved LA-(quad and MC) ICPMS analysis. Mineral Assoc Can Short Course Ser 40:343–348

Hickey K, Bell T (1999) Behaviour of rigid objects during deformation and metamorphism: a test using schists from the Bolton syncline, Connecticut, USA. J Metamorph Geol 17:211–228

Hickmott DD, Shimizu N (1990) Trace element zoning in garnet from the Kwoiek Area, British Columbia: disequilibrium partitioning during garnet growth? Contrib Mineral Petrol 104(6):619–630

Hickmott D, Spear FS (1992) Major-and trace-element zoning in garnets from calcareous pelites in the NW Shelburne Falls Quadrangle, Massachusetts: garnet growth histories in retrograded rocks. J Petrol 33(5):965–1005

Hickmott D, Shimizu N, Spear F, Selverstone J (1987) Trace-element zoning in a metamorphic garnet. Geology 15(6):573–576

Hickmott D, Treves B, Roselle G, Baumgartner L (1997) Micro-PIXE analysis of carbonates and silicates: tracking fluid flow in crustal

environments. Nucl Instrum Methods Phys Res Sect B Beam Interact Mater Atoms 130(1–4):660–665

Holm DK, Selverstone J (1990) Rapid growth and strain rates inferred from synkinematic garnets, Penokean orogeny, Minnesota. Geology 18(2):166–169

Ildefonse B, Sokoutis D, Mancktelow NS (1992) Mechanical interactions between rigid particles in a deforming ductile matrix. Analogue experiments in simple shear flow. J Struct Geol 14(10):1253–1266

Jackson SE, Longerich HP, Dunning GR, Freyer BJ (1992) The application of laser-ablation microprobe inductively coupled plasma-mass spectrometry (LAM-ICP-MS) to in situ trace-element determinations in minerals. Can Mineral 30(4):1049–1064

Janots E, Engi M, Berger A, Allaz J, Schwarz J-O, Spandler C (2008) Prograde metamorphic sequence of REE minerals in pelitic rocks of the Central Alps: implications for allanite-monazite-xenotime phase relations from 250 to 610 °C. J Metamorph Geol 26(5):509–526

Johnson SE (2009) Porphyroblast rotation and strain localization: debate settled!. Geology 37(7):663–666

Johnson S, Dupee M, Guidotti C (2006) Porphyroblast rotation during crenulation cleavage development: an example from the aureole of the Mooselookmeguntic pluton, Maine, USA. J Metamorph Geol 24(1):55–73

Jung S, Hellebrand E (2006) Trace element fractionation during high-grade metamorphism and crustal melting—constraints from ion microprobe data of metapelitic, migmatitic and igneous garnets and implications for Sm-Nd garnet chronology. Lithos 87(3):193–213

Kelly E, Carlson W, Connelly J (2011) Implications of garnet resorption for the Lu-Hf garnet geochronometer: an example from the contact aureole of the Makhavinekh Lake Pluton, Labrador. J Metamorph Geol 29(8):901–916

Kessel R, Schmidt MW, Ulmer P, Pettke T (2005) Trace element signature of subduction-zone fluids, melts and supercritical liquids at 120–180 km depth. Nature 437(7059):724

Kohn MJ (2004) Oscillatory- and sector-zoned garnets record cyclic (?) rapid thrusting in central Nepal. Geochem Geophys Geosyst 5(12):1–9

Kohn MJ (2009) Models of garnet differential geochronology. Geochim Cosmochim Acta 73(1):170–182

Kohn MJ, Malloy MA (2004) Formation of monazite via prograde metamorphic reactions among common silicates: implications for age determinations. Geochim Cosmochim Acta 68(1):101–113

Kohn MJ, Corrie SL, Markley C (2015) The fall and rise of metamorphic zircon. Am Mineral 100(4):897–908

Konrad-Schmolke M, O'Brien PJ, de Capitani C, Carswell DA (2008) Garnet growth at high-and ultra-high pressure conditions and the effect of element fractionation on mineral modes and composition. Lithos 103(3):309–332

Lanzirotti A (1995) Yttrium zoning in metamorphic garnets. Geochim Cosmochim Acta 59(19):4105–4110

Le Fort P (1975) Himalayas: the collided range. Present knowledge of the continental arc. Am J Sci 275(1):44

Martin AJ (2009) Sub-millimeter heterogeneity of yttrium and chromium during growth of semi-pelitic garnet. J Petrol 50(9):1713–1727

Menard T, Spear FS (1996) Interpretation of plagioclase zonation in calcic pelitic schist, south Strafford, Vermont, and the effects on thermobarometry. Can Mineral 34(1):133–146

Mohan A, Windley B, Searle M (1989) Geothermobarometry and development of inverted metamorphism in the Darjeeling-Sikkim region of the eastern Himalayan. J Metamorph Geol 7(1):95–110

Moore S, Carlson W, Hesse M (2013) Origins of yttrium and rare earth element distributions in metamorphic garnet. J Metamorph Geol 31(6):663–689

Mottram CM, Argles T, Harris N, Parrish R, Horstwood M, Warren C, Gupta S (2014a) Tectonic interleaving along the Main Central Thrust, Sikkim Himalaya. J Geol Soc 171(2):255–268

Mottram CM, Warren CJ, Regis D, Roberts NM, Harris NB, Argles TW, Parrish RR (2014b) Developing an inverted Barrovian sequence; insights from monazite petrochronology. Earth Planet Sci Lett 403:418–431

Mukhopadhyay DK, Chakraborty S, Trepmann C, Rubatto D, Anczkiewicz R, Gaidies F, Dasgupta S, Chowdhury P (2017) The nature and evolution of the Main Central Thrust: structural and geochronological constraints from the Sikkim Himalaya, NE india. Lithos 282:447–463

Müller W, Aerden D, Halliday AN (2000) Isotopic dating of strain fringe increments: duration and rates of deformation in shear zones. Science 288(5474):2195–2198

Norman M, Pearson N, Sharma A, Griffin W (1996) Quantitative analysis of trace elements in geological materials by laser ablation ICPMS: instrumental operating conditions and calibration values of NIST glasses. Geostand Geoanal Res 20(2):247–261

Passchier C, Trouw R, Zwart H, Vissers R (1992) Porphyroblast rotation: eppur si muove? J Metamorph Geol 10(3):283–294

Paterson S, Vernon R (2001) Inclusion trail patterns in porphyroblasts from the Foothills Terrane, California: a record of orogenesis or local strain heterogeneity? J Metamorph Geol 19(4):351–372

Paton C, Hellstrom J, Paul B, Woodhead J, Hergt J (2011) Iolite: freeware for the visualisation and processing of mass spectrometric data. J Anal At Spectrom 26(12):2508–2518

Paul B, Paton C, Norris A, Woodhead J, Hellstrom J, Hergt J, Greig A (2012) Cellspace: a module for creating spatially registered laser ablation images within the Iolite freeware environment. J Anal At Spectrom 27(4):700–706

Pearce NJ, Perkins WT, Westgate JA, Gorton MP, Jackson SE, Neal CR, Chenery SP (1997) A compilation of new and published major and trace element data for NIST SRM 610 and NIST SRM 612 glass reference materials. Geostand Newslett 21(1):115–144

Pyle JM, Spear FS (1999) Yttrium zoning in garnet: coupling of major and accessory phases during metamorphic reactions. Geol Mater Res 1(6):1–49

Pyle JM, Spear FS, Rudnick RL, McDonough WF (2001) Monazite–xenotime–garnet equilibrium in metapelites and a new monazite–garnet thermometer. J Petrol 42(11):2083–2107

Raimondo T, Payne J, Wade B, Lanari P, Clark C, Hand M (2017) Trace element mapping by LA-ICP-MS: assessing geochemical mobility in garnet. Contrib Mineral Petrol 172(4):17

Rocholl A (1998) Major and trace element composition and homogeneity of microbeam reference material: basalt glass USGS BCR-2G. Geostand Newslett 22(1):33–45

Rosenfeld JL (1970) Rotated garnets in metamorphic rocks. Geol Soc Am Spec Pap 129:1–102

Schoneveld C (1977) A study of some typical inclusion patterns in strongly paracrystalline-rotated garnets. Tectonophysics 39(1–3):453–471

Skora S, Baumgartner LP, Mahlen NJ, Johnson CM, Pilet S, Hellebrand E (2006) Diffusion-limited REE uptake by eclogite garnets and its consequences for Lu-Hf and Sm-Nd geochronology. Contrib Mineral Petrol 152(6):703–720

Skora S, Lapen TJ, Baumgartner LP, Johnson CM, Hellebrand E, Mahlen NJ (2009) The duration of prograde garnet crystallization in the UHP eclogites at Lago di Cignana, Italy. Earth Planet Sci Lett 287(3–4):402–411

Smit MA, Scherer EE, Mezger K (2013) Lu-Hf and Sm-Nd garnet geochronology: chronometric closure and implications for dating petrological processes. Earth Planet Sci Lett 381:222–233

Spear FS, Selverstone J, Hickmott D, Crowley P, Hodges KV (1984) PT paths from garnet zoning: a new technique for deciphering tectonic processes in crystalline terranes. Geology 12(2):87–90

Stowell HH, Menard T, Ridgway CK (1996) Ca-metasomatism and chemical zonation of garnet in contact-metamorphic aureoles, Juneau Gold Belt, southeastern Alaska. Can Mineral 34(6):1195–1209

Stüwe K (1997) Effective bulk composition changes due to cooling: a model predicting complexities in retrograde reaction textures. Contrib Mineral Petrol 129(1):43–52

Tiller WA (1991) The science of crystallization: macroscopic phenomena and defect generation. Cambridge University Press, Cambridge

Ulrich T, Kamber BS, Jugo PJ, Tinkham DK (2009) Imaging element-distribution patterns in minerals by laser ablation-inductively coupled plasma-mass spectrometry (LA-ICP-MS). Can Mineral 47(5):1001–1012

Viete DR, Lister GS (2016) On the significance of short-duration regional metamorphism. J Geol Soc 174:377–392

Watson EB (1996) Surface enrichment and trace-element uptake during crystal growth. Geochim Cosmochim Acta 60(24):5013–5020

Watson EB, Liang Y (1995) A simple model for sector zoning in slowly grown crystals: implications for growth rate and lattice diffusion, with emphasis on accessory minerals in crustal rocks. Am Mineral 80(11–12):1179–1187

Watson EB, Müller T (2009) Non-equilibrium isotopic and elemental fractionation during diffusion-controlled crystal growth under static and dynamic conditions. Chem Geol 267(3):111–124

Woodhead JD, Hellstrom J, Hergt JM, Greig A, Maas R (2007) Isotopic and elemental imaging of geological materials by laser ablation inductively coupled plasma-mass spectrometry. Geostand Geoanal Res 31(4):331–343

Yang P, Pattison D (2006) Genesis of monazite and Y zoning in garnet from the Black Hills, South Dakota. Lithos 88(1):233–253

Yang P, Rivers T (2001) Chromium and manganese zoning in pelitic garnet and kyanite: spiral, overprint, and oscillatory (?) zoning patterns and the role of growth rate. J Metamorph Geol 19(4):455–474

Yang P, Rivers T, Jackson S (1999) Crystal-chemical and thermal controls on trace-element partitioning between coexisting garnet and biotite in metamorphic rocks from western Labrador. Can Mineral 37(2):443–468

Zhao G, Wilde SA, Cawood PA, Lu L (2000) Petrology and P–T path of the Fuping mafic granulites: implications for tectonic evolution of the central zone of the North China Craton. J Metamorph Geol 18(4):375–391

Zulauf G, Helferich S (1997) Strain and strain rate in a synkinematic trondhjemitic dike: evidence for melt-induced strain softening during shearing (Bohemian Massif, Czech Republic). J Struct Geol 19(5):639–652